Journal of Materials Chemistry C

Back in bismuth: Controlling triplet energy transfer, phosphorescence, and radioluminescence via supramolecular interactions

Journal:	*Journal of Materials Chemistry C*
Manuscript ID	TC-ART-06-2023-002040.R3
Article Type:	Paper
Date Submitted by the Author:	16-Sep-2023
Complete List of Authors:	Marwitz, Alexander; Georgetown University, Department of Chemistry Nicholas, Aaron; The Pacific Northwest National Laboratory Thapa Magar, Rajani; University of New Mexico, Chemistry and Chemical Biology Dutta, Anuj; Georgetown University, Department of Chemistry Swanson, Joel; Georgetown University Hartman, Tyler; Georgetown University, Department of Chemistry Bertke, Jeffery; Georgetown University, Department of Chemistry Rack, Jeffrey; University of New Mexico, Chemistry and Chemical Biology Jacobsohn, Luiz; Clemson University Knope, Karah; Georgetown University, Department of Chemistry

Back in bismuth: Controlling triplet energy transfer, phosphorescence, and radioluminescence via supramolecular interactions

Alexander C. Marwitz,[1] Aaron D. Nicholas,[2] Rajani Thapa Magar,[4] Anuj K. Dutta,[1] Joel Swanson,[1] Tyler Hartman,[1] Jeffery A. Bertke,[1] Jeffrey J. Rack,[4] Luiz G. Jacobsohn,[3] Karah E. Knope[1,]*

1 Department of Chemistry, Georgetown University, Washington, D.C. 20057, United States of America
2 National Security Directorate, Pacific Northwest National Laboratory, 902 Battelle Boulevard, Richland, WA 99354, United States of America
3 Department of Materials Science and Engineering, Clemson University, Clemson, SC 29634, United States of America
4 Department of Chemistry and Chemical Biology, University of New Mexico, Albuquerque, NM 87111, United States of America

KEYWORDS Bismuth; radioluminescence; luminescence; phosphorescence; electronic structure calculations; supramolecular interactions; electron transfer; triplet energy transfer

ABSTRACT

Five bismuth(III)-organic phases that consist of supramolecular assemblies of Bi-2,6-pyridinedicarboxylate structural units and substituted 1,10-phenanthroline molecules (R-Phen; R = H, 5-methyl, 5-chloro, 2,9-dimethyl, and 2,9-dicholoro) were synthesized. All five compounds exhibited solid-state photoluminescence. Whereas the phases containing 2,9-dimethylphenanthroline (Me_2Phen) and 2,9-dichlorophenanthroline (Cl_2Phen) displayed solely phosphorescence, the structures built from 5-methylphenanthroline and 5-chlorophenanthroline showed exclusively fluorescence. The remaining phase,

consisting of phenanthrolinium, exhibited both fluorescence and phosphoresence. It was determined that phosphorescence arises from triplet state emission ($T_1 \rightarrow S_0$) of substituted R-Phen units while fluorescence originates from Bi(III) coordinated pyrdinedicarboxylate ligands. Bismuth induces spin-orbit coupling for triplet state population and additionally acts as a heavy metal attenuator for X-ray luminescence (radioluminescence). The electronic structure was mapped and excitation pathway investigated via density functional theory calculations. Computational findings indicate favorable conditions for triplet energy transfer from donor Bi(III)-organic units to acceptor R-Phen derivatives. It is proposed that for the phosphorescent compounds, strong π-π interactions promote electron transfer, whereas the compounds that exhibit purely fluorescence lack any such π-π interactions and undergo triplet energy transfer. These results provide a useful platform for probing structure-property relationships of luminescent bismuth-organic compounds, and specifically highlights the role of noncovalent interactions in achieving room temperature phosphorescence and radioluminescence.

INTRODUCTION

Materials with stable and attainable triplet excited states are important for applications such as photocatalysis,[1-4] electronic displays,[5-9] and sensors.[10-12] A variety of methods have been used to achieve triplet state excitation. Historically, heavy atoms (i.e. late transition metals) have been utilized alongside aromatic organic compounds to induce enhanced spin-orbit coupling and increase rates of intersystem crossing.[13] While this method is effective at populating triplet excited states, the increased rates of

intersystem crossing lead to short excited state lifetimes and inherently reduce the rate of single electron transfer for photocatalysis.[14] Furthermore, these metal-organic compounds often produce metal-to-ligand charge transfer (MLCT) states that display valuable luminescent properties, but are not easily controlled.[15]

Recent developments in triplet sensitization of organic molecules have exploited the phenomenon of triplet energy transfer (TET).[16-18] The theory surrounding TET is built from the concept of Dexter energy transfer (DET), which was first proposed in 1953.[19, 20] Essentially, the process involves the non-radiative transfer of energy from the triplet excited state of a donor molecule (^{3}D*) to the ground state of an acceptor (A), resulting in the triplet excited acceptor (^{3}A*). TET can follow a concerted Dexter-like process but can also occur via a stepwise charge transfer-mediated state.[17] The result of this process is the population of the triplet excited state of an acceptor molecule, displaying long-lived lifetimes due to the slow rate of electron transfers. There are numerous examples of TET materials inducing photochemical reactions.[21, 22] However, most current TET materials are either solution-based or built from semiconductor nanocrystal/quantum dot hosts, with an interfacial energy transfer to an acceptor in the matrix outside the host material.[23] There are relatively fewer examples of TET occurring in crystalline molecular solids. As an example, TET was observed for single crystals of diphenyl doped with trace impurities of naphthalene or phenanthrene, wherein the diphenyl sensitized the triplet state emission of the dopant.[24] Attaining such efficient TET in single crystalline materials where the emission is dictated solely by the identity of the guest molecule could result in a new path toward the design of electronic displays and other solid-state lighting devices.

In recent years, there has been a push to design materials derived from globally abundant, environmentally benign, and non-toxic elements. Many current luminescent materials involve the use of metals with environmentally taxing separations techniques (i.e. the rare earths)[25], notable toxicity (i.e. CdS quantum dots)[26], or low crustal abundance and high cost such as iridium and platinum (often used in organic light emitting diodes).[27] To this end, bismuth is an ideal candidate for materials design: it is a by-product of lead ore processing, it has low- to non-toxicity, and it is relatively abundant and cheap. Moreover, bismuth(III) is a closed-shell metal ion like the d^{10} metals, with literature precedence for fluorescence and phosphorescence.[28-33] Bismuth(III)-organic materials have been shown to exhibit MLCT, as well as halide-metal to ligand charge transfer (XMLCT) wherein the bismuth-halide subunit is involved in the excitation process; emission from these compounds has been observed over the visible region.[34-36] Luminescence deriving from the forbidden $^3P_0 \rightarrow {}^1S_0$ transition of the $6s^2$ electrons has also been reported and exhibits broad emission in the blue-green region.[37] Additionally, bismuth provides other benefits over the metals used in current luminescent materials. It is a good heavy metal attenuator for X-ray absorption; this can lead to radioluminescence which has applications in imaging and sensing.[38, 39] Furthermore, the $6s^2$ lone pair (LP) can exhibit varying degrees of stereochemical activity and thereby provide rich coordination chemistry as well as access to additional noncovalent interactions such as LP-π interactions.[40]

In our previous work, we reported on a bismuth(III)-organic compound that displayed triplet state emission from 1,10-phenanthrolinium (PhenH).[41] This compound displayed remarkable properties

including a long luminescent lifetime, as well as color tuning through small-quantity doping of trivalent lanthanides. While the supramolecular interactions including hydrogen-bonding, π-π interactions, and LP-π interactions were clearly important for reducing molecular vibrations and quenching of the triplet state, the role of specific interactions on the observed luminescence was unclear. Towards this end, in this work supramolecular assemblies consisting of Bi-pyridinedicarboxylate complexes and judiciously selected substituted phenanthrolines were prepared to study the effects of noncovalent interactions on the photophysical properties, governed in part by ligand electronics and sterics. The result is a family of structurally related materials, with subtle changes at the Bi-organic moiety and organic R-Phen units but different supramolecular interactions. The photophysical properties are explored using temperature variable luminescence as well as UV-vis and radioluminescence spectroscopies. Spectroscopic results are interpreted using computational density functional theory (DFT) by mapping the electronic structure, predicting the excitation pathway, and determining the changes in free energy of an electron transfer. This work provides insights into the structure-property relationships of bismuth-organic compounds towards achieving fluorescence, phosphorescence, and radioluminescence, allowing for controllable emissive properties through subtle synthetic alterations.

RESULTS AND DISCUSSION

Synthetic Details

It is well established that bismuth(III)-organic compounds can be difficult to synthesize due to the poor solubility of bismuth(III) starting materials as well as the hydrolytic instability of bismuth.[42] Hydrothermal conditions are frequently utilized to overcome solubility issues; however, in this work any attempts to use such conditions led to the formation of a previously published Bi-PDC coordination polymer,

$[Bi(HPDC)(PDC)\cdot H_2O]_n$, where PDC is 2,6-pyridinedicarboxylate.[43] For several of the syntheses, stirring at room temperature yielded phase pure powders, but solvent layering was utilized to acquire diffraction-quality single crystals for each compound.

In an effort to examine the impact of structural modifications on the luminescent behavior of Bi-organic compounds, we sought to utilize 1,10-phenanthroline derivatives with substitutions on the "front" at the 2,9-positions, as well as substitutions on the "back" in the 5-position (Fig. 1). It was expected that structural changes from the previously published PhenH compound, $PhenH[Bi_2(HPDC)_2(PDC)_2(NO_3)]\cdot 4H_2O$, would occur due to increased steric effects. Further, by using both weakly electron donating and electron withdrawing substituents, changes to supramolecular interactions like π-π stacking and hydrogen bonding were expected to occur, allowing for the isolation of the effect of each interaction on the observed properties.

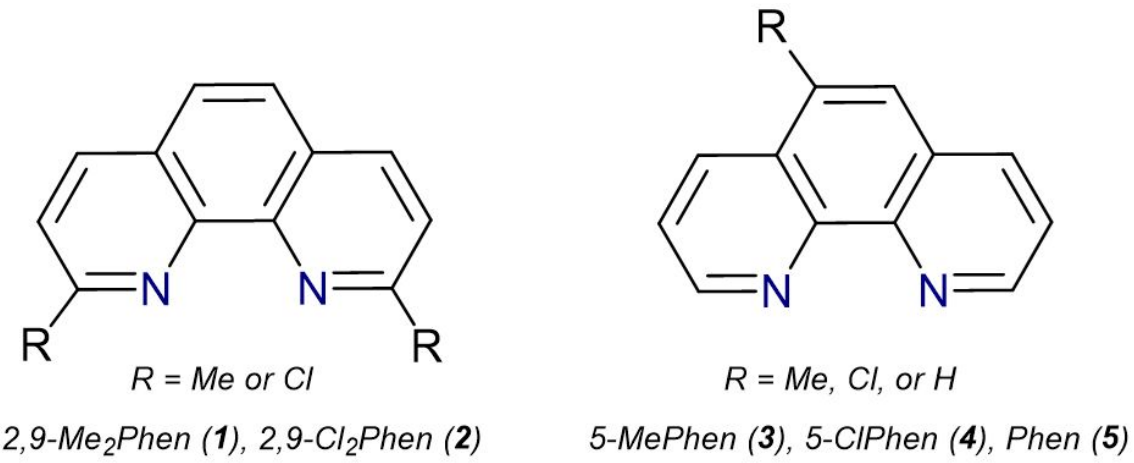

Fig. 1. Substituted 1,10-phenanthrolines used in this study. The number in parentheses corresponds to the compound number with which it was utilized.

Structure Descriptions

All five compounds consist of a dimeric bismuth structural unit bridged through the carboxylates of two PDC ligands. Compounds **1**, **2**, and **5** display π-π stacking interactions between an inner coordination PDC and the outer coordination R-Phen, while **3** and **4** do not. However, all five compounds contain significant hydrogen bonding interactions. The noncovalent interactions for each compound are summarized in Tables S1-S5.

2,9-Me_2PhenH[$Bi_2(HPDC)_2(PDC)_2(NO_3)$]·$4H_2O$ (1)

Compound **1** is built from two crystallographically unique bismuth ions that are bridged through the carboxylates of two doubly-deprotonated PDC ligands into dimeric complexes as shown in Fig. 2. Each bismuth ion is further chelated by a tridentate, singly-deprotonated HPDC ligand. One bismuth of the dimeric unit is nine-coordinate, exhibiting a holodirected coordination geometry with a η^2-nitrate capping the coordination sphere. The other bismuth ion is seven-coordinate, exhibiting a hemidirected coordination geometry with an open coordination face indicative of a stereochemically active $6s^2$ lone pair. The Bi-O distances range from 2.309(5) to 2.846(7) Å for the nine-coordinate bismuth and 2.200(5) to 2.630(5) Å for the seven-coordinate bismuth. The Bi-N_{PDC} bond distances show much less variability with a range of 2.413(6) to 2.461(4) Å and the Bi---Bi distance is 4.163(3) Å. A moderate hydrogen bond exists between the nitrate (acceptor) and the 2,9-Me_2PhenH (donor) with a N-H···O distance of 2.738(8) Å and N-H···O

angle of 144(8)˚. The C-N-C angles for 2,9-Me_2PhenH are 123.3(7)˚ and 117.5(7)˚ and are consistent with reported values for a protonated and deprotonated nitrogen on 1,10-phenanthroline, respectively, confirming the charge of the Me_2PhenH ion.[44] Furthermore, there is evidence of a strong lone pair- π (LP-π) interaction between the bismuth $6s^2$ lone pair and the Me_2PhenH, with a Bi-Cg_{Phen} distance of 3.636 Å and a β angle of 12.96˚.

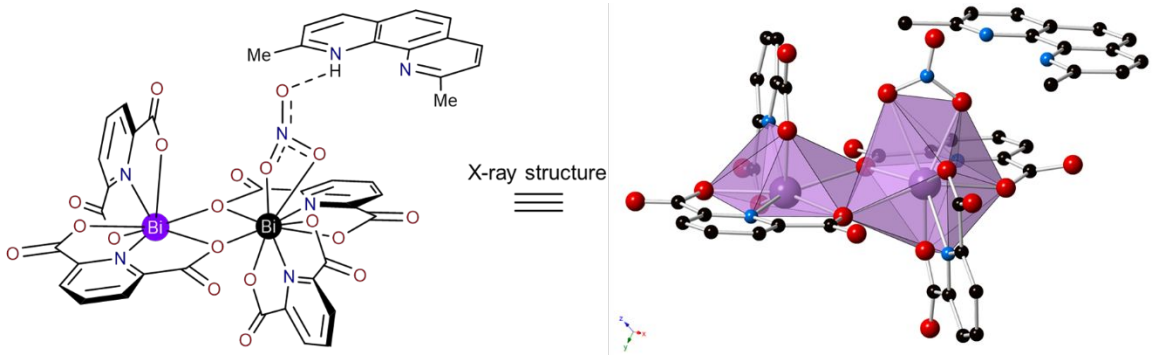

Fig. 2. Left: Illustration of **1**. The seven-coordinate bismuth center is highlighted in purple and the nine-coordinate Bi center is shown in black. Right: Polyhedral representation of the dimeric unit in **1**. Purple = bismuth, blue = nitrogen, red = oxygen, and black = carbon atoms. Hydrogen atoms and lattice water molecules have been omitted for clarity.

As shown in Figure S6, the $Bi_2(HPDC)_2(PDC)_2(NO_3)$ dimeric units propagate into 1-D chains via PDC···2,9-Me_2PhenH···PDC π-π stacking interactions. The strongest π-π stacking interactions occur between 2,9-Me_2PhenH and PDC rings and exhibit centroid···centroid distances (Cg_{Phen}···Cg_{PDC}) ranging from 3.611(4) to 3.690(4) Å with slip angles of 12.8° and 22.3°, respectively. Note that only those π-π interactions < 4.0 Å were considered significant following literature precedence;[45, 46] the closest PDC--PDC π-π interaction on adjacent dimers was 4.445(4) Å. The 1-D chains are further connected into a 3-D supramolecular structure via a significant hydrogen bonding network as shown in Figure S7. The hydrogen

bond strengths range from weak to strong and exist between the carboxylates of the PDC and the lattice water molecules with O-H···O distances ranging from 2.436(8) to 2.877(8) Å. Typical O-H···O angles for weak interactions were 144(8)˚ and for strong interactions were 172(10)˚.

2,9-Cl$_2$Phen[Bi$_2$(HPDC)$_2$(PDC)$_2$(H$_2$O)]·4H$_2$O (2)

Compound **2** is built from the same $Bi_2(HPDC)_2(PDC)_2$ dimeric unit as that described for **1**; however, the formerly nine-coordinate bismuth ion that was bound to an anionic nitrate is an eight-coordinate bismuth site bound to a neutral water molecule (Fig. 3). Moreover, there is less variability in the Bi-O bond distances as compared to **1**; Bi-O distances range from 2.268(4) to 2.671(4) Å for the eight-coordinate bismuth ion and 2.206(4) to 2.648(4) Å for the seven-coordinate bismuth site. The Bi-N_{PDC} distances range from 2.413(4) and 2.446(5) Å, and the Bi---Bi distance is 4.159(9) Å. As a consequence of the neutral water substituent instead of a nitrate, the outer coordination 2,9-Cl_2Phen is deprotonated. The C-N-C bond angles of 115.5(5)˚ and 116.5(5)˚ are consistent with literature values of deprotonated phenanthroline derivatives. As shown in Figure 3, the 2,9-Cl_2Phen engages in hydrogen bonding interactions with the bound water molecule, forming an O-H···N interaction rather than the N-H···O interaction observed in **1**. The D···A distance is 2.924(7) Å the O-H···N angle is 137(5)˚. As with **1**, there is evidence of a LP-π interaction between the bismuth $6s^2$ lone pair and the Cl_2Phen, with a Bi-Cg_{Phen} distance of 3.714 Å and a β angle of 19.36˚.

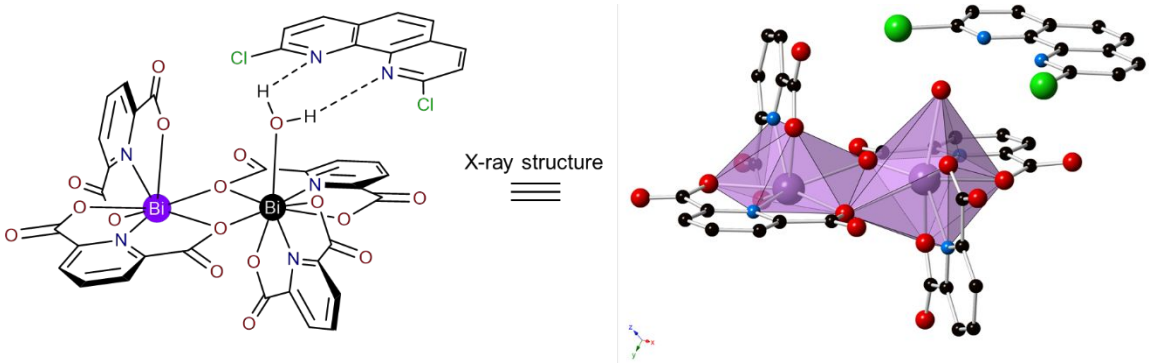

Fig. 3. Left: Illustration of **2**. The seven-coordinate bismuth center is highlighted in purple and the eight coordinate bismuth center is shown in black. Right: Polyhedral representation of the dimeric unit in **2**. Purple = bismuth, blue = nitrogen, red = oxygen, black = carbon, and green = chloride atoms. Hydrogen atoms and lattice water molecules have been omitted for clarity.

As in **1**, the $Bi_2(HPDC)_2(PDC)_2(H_2O)$ dimers in **2** are connected through strong PDC···2,9-Cl_2Phen···PDC π-π interactions to create 1-D supramolecular chains (Figure S8), with centroid···centroid distances of 3.562(3) and 3.600(3) Å and slip angles of 12.4˚ and 17.7˚, respectively. The 1-D chains are further connected into a 3-D supramolecular structure (Figure S9) through an extensive hydrogen bonding network that forms via PDC carboxylate O atoms and lattice water molecules. The O-H···O distances range from 2.450(5) to 2.934(5) Å, with O-H···O angles between 153(5)˚ and 179(6)˚.

$(5\text{-MePhenH})_2[Bi_2(HPDC)_2(PDC)_2(NO_3)_2]\cdot 6H_2O$ (3)

Compound **3** consists of one crystallographically unique bismuth ion. As shown in Figure 4, the metal center is bridged through two carboxylate O atoms from two doubly-deprotonated PDC ligands to a symmetry equivalent bismuth ion. The bismuth ions are further chelated by a tridentate, singly-deprotonated HPDC ligand and form the $Bi_2(HPDC)_2(PDC)_2$ dimeric units described for **1** and **2**. Each bismuth ion is

also coordinated to a η^2-nitrate hence yielding two nine-coordinate metal centers with holodirected coordination geometries and stereochemically inactive lone pairs. The Bi-O distances range from 2.218(2) to 3.023(4) Å; the longest Bi-O bond occurs between bismuth and one of the nitrate oxygen atoms. The wide range in distances implies a degree of asymmetry around the metal center that is perhaps induced by a weakly bound nitrate. The Bi-N_{PDC} distances are 2.433(2) Å and 2.468(2) Å and the Bi--Bi distance within the dimeric unit is 4.247(8) Å. The nitrate (acceptor) forms a strong hydrogen bonding interaction with an outer coordination sphere 5-MePhenH (donor) that lies perpendicular to the plane of the bismuth-PDC scaffold. The N-H···O distance is 2.795(3) Å with a N-H···O angle of 159°.

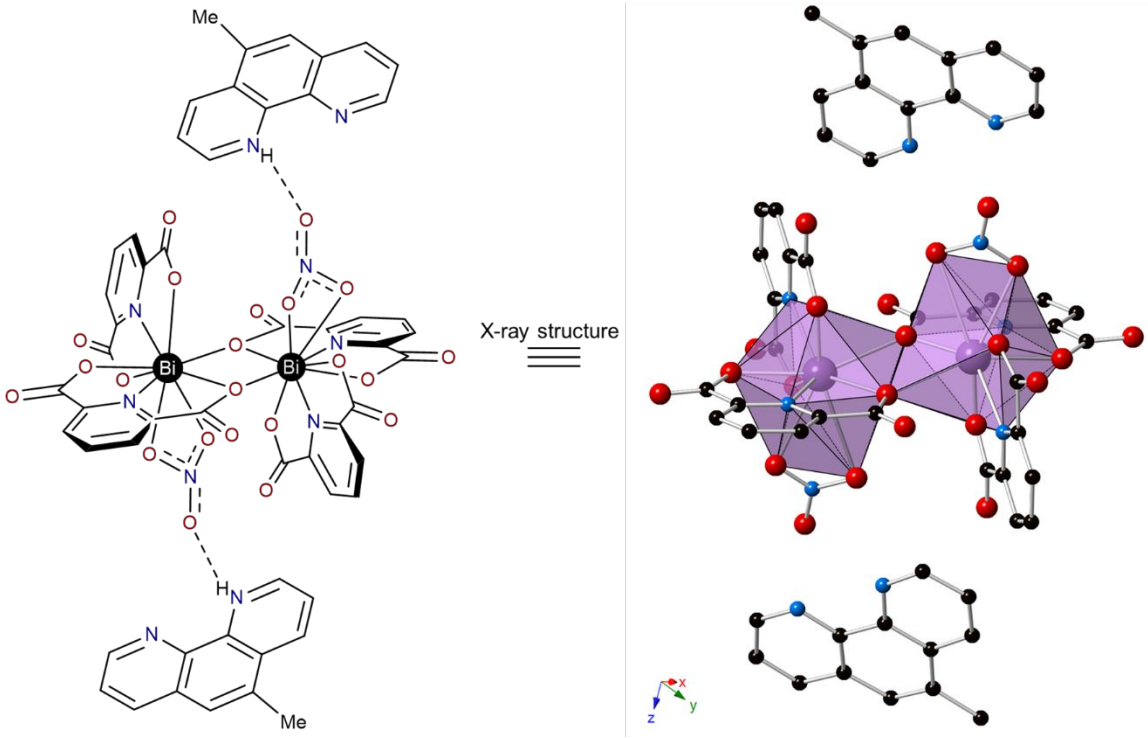

Fig. 4. Left: Illustration of **3** with the two nine-coordinate bismuth sites shown in black. Right: Polyhedral representation of the dimeric unit in **3**. Purple = bismuth, blue = nitrogen, red = oxygen, and black = carbon atoms. Hydrogen atoms and lattice water molecules have been omitted for clarity.

Unlike our previous report on [PhenH][$Bi_2(HPDC)_2(PDC)_2(NO_3)$] and the structures of **1** and **2**, there are no significant π-π interactions between PDC and 5-MePhenH, nor between PDC rings on neighboring dimers. In fact, the only notable π-π interactions exist between neighboring 5-MePhenH rings (Fig. S10) with a centroid···centroid distance of 3.470(2) Å and slip angle of 15.3˚. Nonetheless, these interactions together with an extensive hydrogen bonding network result in an overall 3-D supramolecular structure. The hydrogen bonding network forms via the lattice water molecules and the carboxylic acid of the HPDC which act as hydrogen bond donors, and lattice water molecules, carboxylates of PDCs, and the nitrate that act as hydrogen bond acceptors; O-H···O distances range from 2.517(3) to 2.988(3) Å.

(5-ClPhenH)$_2$[Bi$_2$(HPDC)$_2$(PDC)$_2$(NO$_3$)$_2$]·6H$_2$O (4)

Compound **4** is isomorphous to **3**. The structure consists of the same $Bi_2(HPDC)_2(PDC)_2(NO_3)_2$ dimeric scaffold with two nine-coordinate, holodirected bismuth ions bridged through PDC ligands (Fig. 5). The Bi-O distances range from 2.215(2) to 3.040(5) Å, and the Bi-N_{PDC} distances are 2.429(3) Å and 2.457(2) Å. The Bi--Bi distance within the dimeric unit is 4.240(10) Å. The nitrate (acceptor) forms a strong hydrogen bonding interaction with an outer coordination sphere 5-ClPhenH (donor) that lies perpendicular to the plane of the bismuth-PDC molecules. The N-H···O distance is 2.780(4) Å with a N-H···O angle of 163(3)˚.

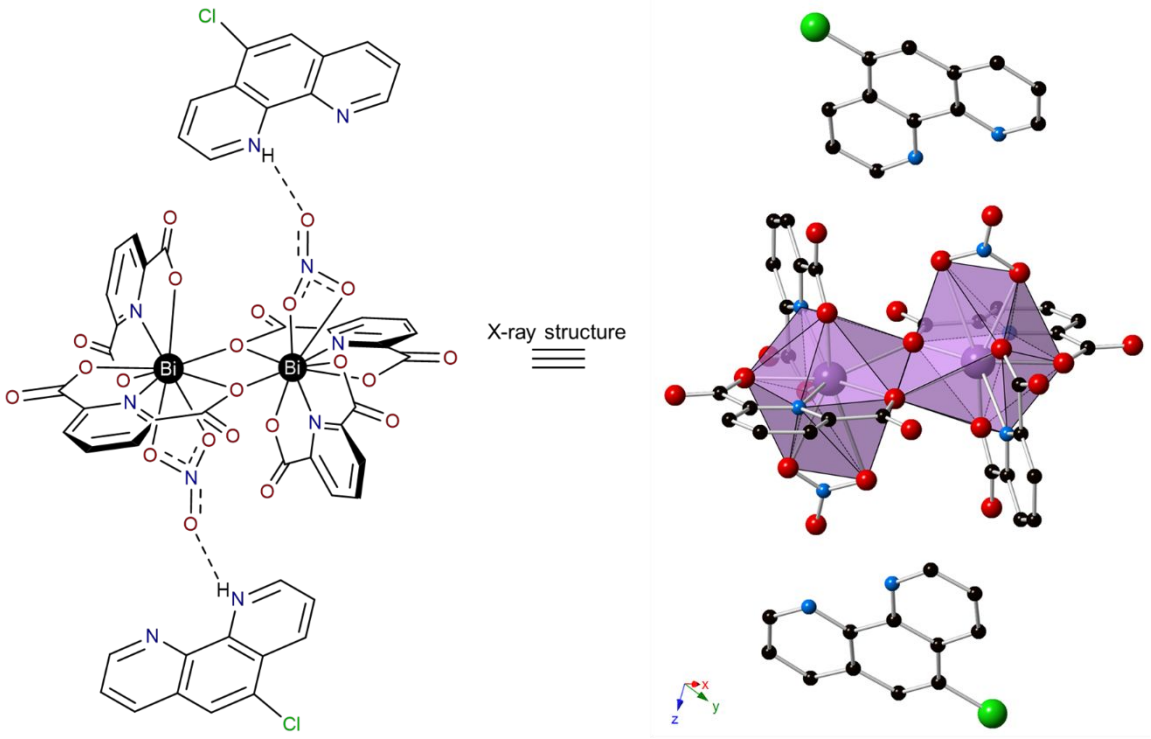

Fig. 5. Left: Illustration of **4**. Right: Polyhedral representation of the dimeric unit in **4**. Purple = bismuth, blue = nitrogen, red = oxygen, black = carbon, and green = chloride atoms. Hydrogen atoms and lattice water molecules have been omitted for clarity.

As with compound **3**, there are no significant π-π interactions between PDC and 5-ClPhenH, nor between PDC rings on neighboring dimers. However, as shown in Figure S11, the 5-ClPhenH form π-π stacking interactions along the [100] with a centroid···centroid distance of 3.492(2) Å and slip angle of 17.3˚. These interactions together with an extensive hydrogen bonding network similarly result in an overall 3-D supramolecular structure (Table S4). Lattice water molecules and the carboxylic acid of the HPDC act as hydrogen bond donors, while the lattice water molecules, carboxylates of PDCs, and the nitrate act as hydrogen bond acceptors; O-H···O distances range from 2.494(3) to 2.965(3) Å.

$(PhenH)_2[Bi_2(HPDC)_2(PDC)_2Cl_2]\cdot 8H_2O$ (5)

Compound **5** is built from a similar $Bi_2(HPDC)_2(PDC)_2$ dimeric unit as that described for compounds **1**-**4**. The structure is built from one crystallographically unique bismuth ion that is bound to a chelating HPDC and a bridging PDC. The latter links the Bi site with its symmetry equivalent and yields the dimer shown in Fig. 6A. The bismuth ion is further bound to a chloride ion and thus adopts an eight-coordinate, holodirected coordination geometry. The Bi-Cl distance is 2.8244(7) Å, the Bi-O distances range from 2.297(2) to 2.689(2) Å, and the Bi-N distances are 2.405(2) and 2.512(2) Å. As shown in Figure 6, the PhenH cations engage in hydrogen bonding with the deprotonated carboxylate of the HPDC. The N-H···O distance is 3.129(3) Å with a N-H···O angle of 133(3)˚ (Fig. 6B).

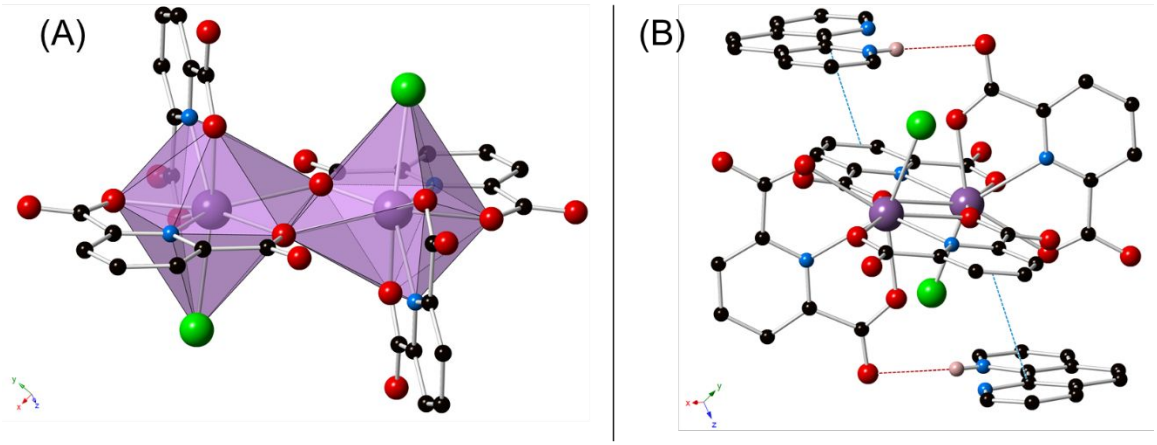

Fig. 6. (A) Polyhedral representation of the $BiCl_2(HPDC)_2(PDC)_2$ dimeric unit observed for **5**. (B) Ball and stick model showing the hydrogen bonding interactions (red dashed lines) between PhenH and HPDC, as well as π-π interactions (blue dashed lines) between PhenH and PDC in **5**. Purple = bismuth, blue = nitrogen, red = oxygen, black = carbon, and green = chloride atoms. Hydrogen atoms and lattice water molecules have been omitted for clarity.

The dimers are further connected into a 1-D chain via PDC···PhenH···PhenH···PDC π-π stacking interactions (Figure S12). The PDC···PhenH interaction has a centroid···centroid distance of 3.772(1) Å and a slip angle of 21.4˚, while the PhenH···PhenH interactions have centroid···centroid distances of

3.701(1) and 3.573(1) Å with slip angles of 25.2˚ and 19.7˚, respectively. Overall, the structure adopts a 3-D supramolecular network through π-π stacking interactions and an extensive hydrogen bonding network that forms between carboxylates on PDC and lattice waters. The O-H···O distances range from 2.476(2) to 2.839(2) Å with O-H···O angles between 163(5)˚ and 179(3)˚.

Photoluminescence

Compounds **1**-**5** are emissive in the solid state upon UV irradiation (Fig. 7). Compound **1** shows green-blue emission at room temperature upon excitation at 380 nm with an emission maximum centered at 500 nm. Vibrationally resolved peaks are also observed at 475 and 535 nm. The emission is similar in energy and profile to that reported previously for $PhenH[Bi_2(HPDC)_2(PDC)_2(NO_3)]\cdot[4H_2O]$, as well as 1,10-phenanthroline phosphorescence at 77 K.[41, 47] The emission of **1** is thus attributed to triplet state emission from Me_2PhenH. This is further evidenced by the long luminescent lifetime of 1769 μs at room temperature (Figure S25). The absolute quantum yield for **1** in the solid state is 28.1±1.1%. An additional excitation peak is observed at 420 nm, yielding the same emission profile, albeit with < 5% of the relative emission intensity (Figure S53). Excitation at less intense local maxima (320 and 365 nm) yield the same emission profile (Figure S54).

Compound **2** emits in the blue region at room temperature upon excitation at 350 nm. The emission profile has a maximum at 490 nm and vibrationally resolved peaks are present at 460 and 525 nm. Overall, the spectrum shows a 10 nm blue shift compared to **1**. The spectrum is consistent with triplet state emission from Cl_2Phen. When excited at 350 nm, the emission at 490 nm has a lifetime of 534 μs (Figure S26). Interestingly, there is a second excitation pathway with a local excitation maximum in the visible region at

420 nm. This leads to identical, albeit less intense, emission as that observed from 350 nm excitation; when excited at 420 nm, the lifetime lowers slightly to 509 μs (Figure S27). The quantum yield for **2** is 9.4±1.0%. As with **1**, excitation at less intense local maxima (290 and 320 nm) yield the same emission profile (Figure S55).

Compounds **3** and **4** display nearly identical excitation and emission spectra. Both compounds exhibit purple emission with a maximum at 430 nm upon excitation at 380 nm. No evidence of vibronic coupling was observed, and the luminescent lifetimes were too short to quantify using our instrument (< 10^{-6} s). These features, coupled with the small Stokes shift seen in the excitation and emission spectra (~50 nm), are consistent with fluorescence from an organic ligand. Based on previous reports of solution-state emission of 2,6-PDC (pH = 6) that show a peak at 430 nm, the emission is attributed to fluorescence from Bi(III) coordinated PDC ligands.[48] It has been demonstrated that the mechanism of spin-orbit coupling enhancement via the external heavy atom effect is purely electronic in nature and involves no vibronic coupling.[49] The loss of vibrational resolution indicates a change in spin-orbit coupling; this may be due to the stereochemically inactive $6s^2$ lone pair in **3** and **4** being tied up in an interaction with the NO_3 capping the coordination sphere, as compared to the stereochemically active lone pair in **1** and **2**. Regardless, **3** and **4** are clearly being influenced differently by the $Bi_2(HPDC)_2(PDC)_2$ subunit than **1** and **2**. Quantum yields were not measured for **3** and **4** due to the small Stokes shift and low emission intensity.

Compound **5** displays blue emission upon excitation at 370 nm. The emission consists of two major features: a broad single peak centered at 405 nm and a group of vibronically coupled peaks at 465, 495, and 530 nm. Lifetime measurements of the peaks reveal a dual fluorescent and phosphorescent behavior. The peak at 405 nm has a short luminescent lifetime (< 10^{-6} s) similar to emission of compounds **3** and **4** and is accordingly assigned to PDC or PhenH fluorescence.[47] The emission at 465 nm exhibits a long lifetime and

is nearly identical to that previously reported by our group, and is ascribed to PhenH phosphorescence.[41]

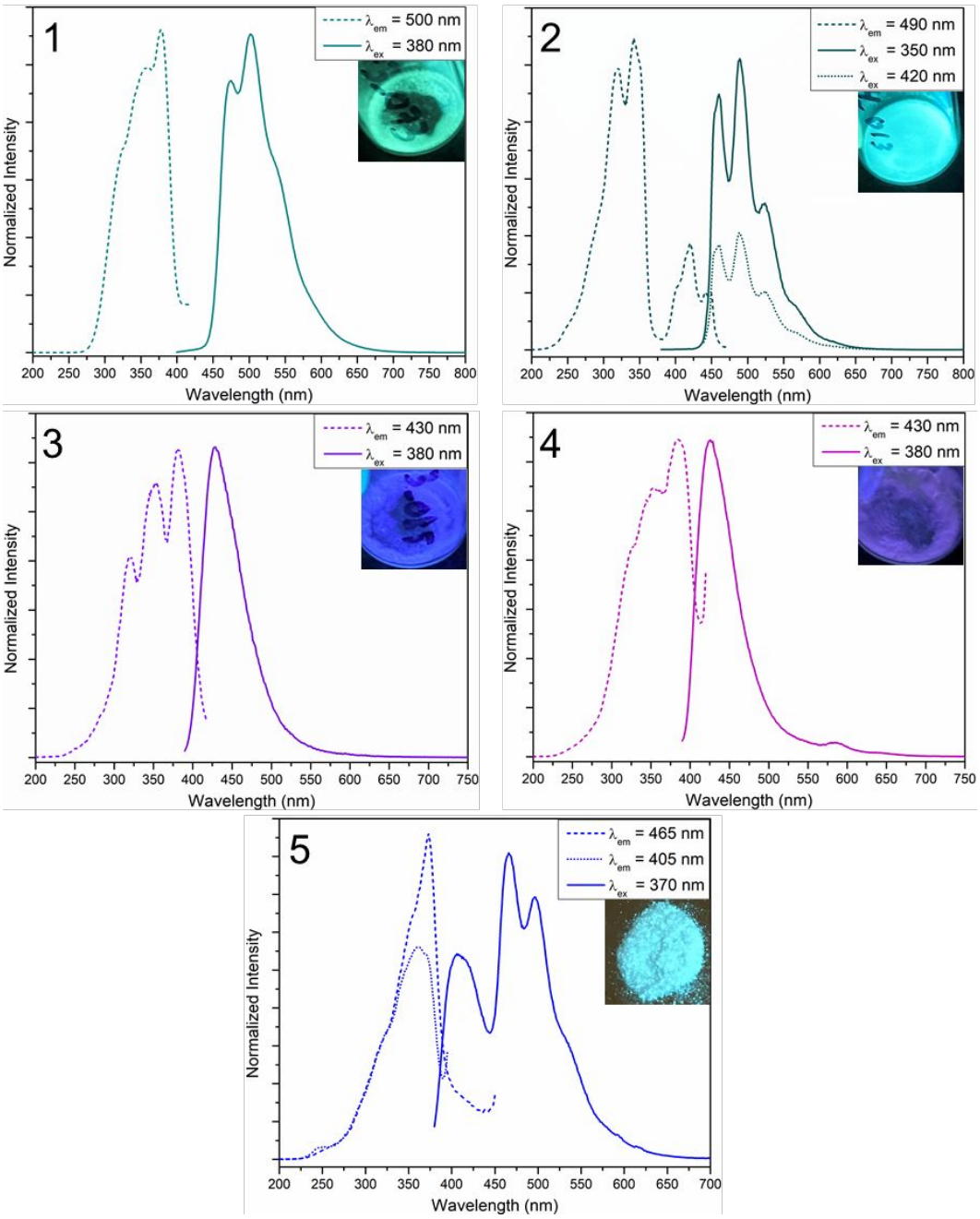

Fig. 7. Solid-state photoluminescence excitation (dashed lines, and dotted line in **5**) and emission (solid lines, and dotted line in **2**) spectra for compounds **1**-**5** collected at room temperature. The insets show a photograph of the material under UV irradiation (λ = 365 nm). Note that for all five compounds, the emission profile did not change significantly upon altering the excitation wavelength used.

Low Temperature Photoluminescence

A notable change in the emission color was observed for compounds **2** and **4** upon immersion in liquid nitrogen. At 77 K, compound **2** shows an expected increase in the splitting of the emission peaks upon excitation between 335-350 nm due to the more resolved vibronic coupling at low temperatures (Fig. 8). Additionally, a new excitation peak grew in at 370 nm. Excitation at 370 nm resulted in no evidence of the previous triplet emission from Cl_2Phen and two new emission peaks are present at 510 and 550 nm. This coincides with a significant color change from blue to green. Further excitation-dependent color tuning could be achieved by exploiting the differences in emission upon excitation at 350 nm and 370 nm at 77 K as shown in Figures S23 and S24.

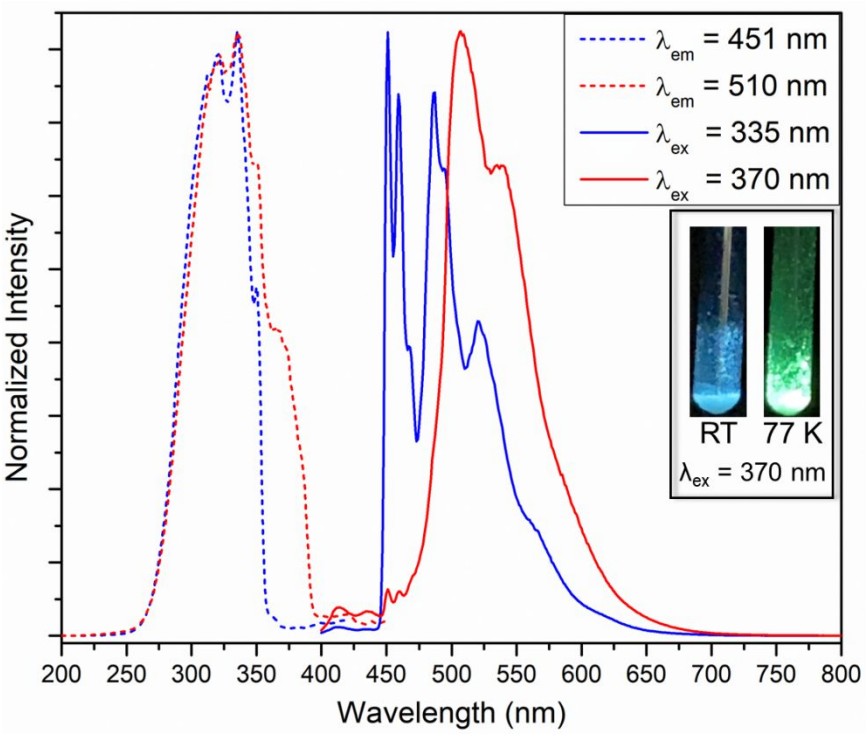

Fig. 8. Low temperature excitation (dashed lines) and emission (solid lines) spectra for compound **2** collected at 77 K. The inset shows the color change of the material upon excitation at 370 nm at room temperature (left) and 77 K (right).

Compound **4** also exhibited a change in the emission spectrum upon cooling to 77 K as displayed in Figure 9. The peak at 430 nm displays vibronically resolved peaks centered at 396, 422, and 440 nm. Additionally, the small shoulder previously seen in the room temperature spectrum at 590 nm grows in significantly, along with a second peak at 540 nm. The peaks have the same excitation maxima as those between 396-440 nm and thus no excitation-dependent color tuning occurs; this suggests that there is significant excited state overlap or 'bleed' between the two bands in **4**. Nonetheless, the emission color changes from violet to a pale pink upon cooling from room temperature to 77 K.

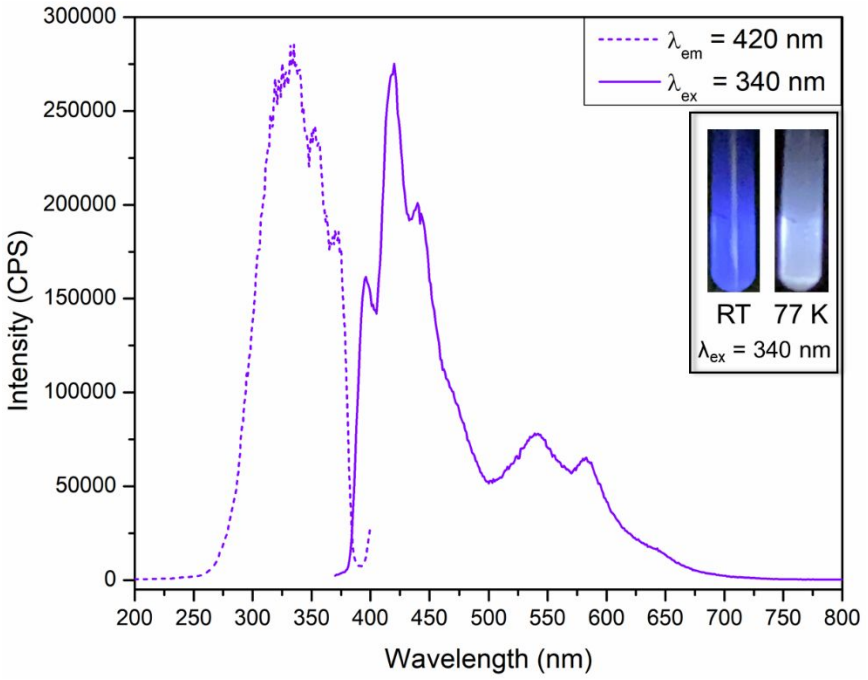

Fig. 9. Solid-state photoluminescence spectra of compound **4** at 77 K. Inset shows photographs of the material at room temperature and 77 K when excited at 340 nm.

Radioluminescence

Compounds **1**, **2** and **5** were found to emit visible light upon X-ray irradiation; however, a suitable quantity of **5** could not be obtained and thus the radioluminescent properties of the compound are not described. The radioluminescence emission spectra for **1** and **2** are shown in Figure 10. The profiles are equivalent to their respective photoluminescence spectra and are consistent with triplet state emission from the phenanthroline

derivatives. To quantify the emission intensity of the radioluminescence, the spectra were integrated between 350 and 750 nm and compared to the integrated area of a commercial standard, bismuth germanium oxide (BGO) powder. Compound **1** showed a relative intensity of 33% compared to BGO, while **2** showed significantly more intensity at 52% relative to BGO.

It is well established that heavy atoms (i.e. bismuth) can absorb ionizing radiation more effectively thus facilitating the radioluminescence process.[38, 39, 50, 51] Notably, **3** and **4** do not show evidence of radioluminescence indicating a disruption in the Bi→Phen energy transfer pathway upon release of a photoelectron in these materials. This strongly suggests that π-π interactions are critical to achieving the phosphorescence and radioluminescence observed for **1**, **2**, and **5**. It is well established that radioluminescence in organic molecules occurs through the interaction of the π electronic structure of the molecule with the charged particle (photoelectron);[52] in this system, the photoelectron is released by bismuth upon interaction with the high energy X-rays. Thus the close bismuth-phen distance induced by the π-π interactions and LP-π interactions may help facilitate the emission from the organic species.

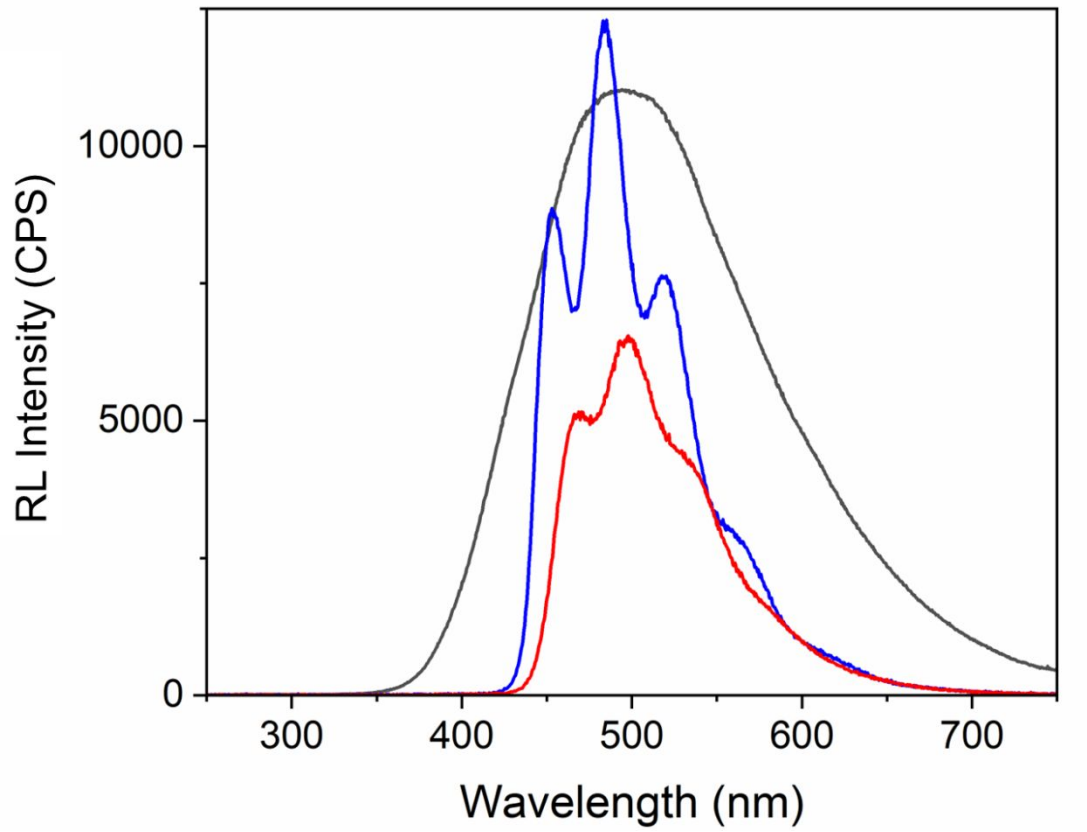

Fig. 10. Radioluminescence spectra of **1** (red) and **2** (blue) compared to a BGO standard (black). The integrated intensities relative to BGO are 33% and 52%, respectively.

Computational Studies

Molecular DFT modelling was performed to determine the electronic structure and resulting photoluminescent behavior observed for **1**-**5**. As noted previously, bismuth-organic compounds readily undergo MLCT or mixed metal/ligand-to-ligand charge transfer under UV excitation.[36, 41, 53, 54] For the compounds reported herein, several energy transfer pathways are plausible including (i) triplet energy transfer, (ii) photoinduced electron transfer, and (iii) isolated R-Phen and PDC $\pi \rightarrow \pi^*$ transitions. To gain

further insight into the pathways and their application to the properties of **1-5**, (i) the electronic structures were mapped, (ii) the electronic transitions of the lowest singlet and triplet states were calculated, and (iii) the thermodynamic favorability for a formal electron transfer was examined.

Electronic Structure and TD-DFT Transitions

As part of this investigation, the electronic structure of **1-5** were first mapped. Density of state calculations were performed and are shown in Figure 11. These states are extracted from the DFT wavefunction and are mapped by molecular orbital construct and energy. For **1-5**, the lower lying unoccupied orbitals are composed of the phen π* molecular orbitals. Generally, these molecular orbitals energetically sit below the PDC π* and well below the empty Bi 6p orbitals; only **2** is the exception. The higher lying occupied molecular orbitals consist of those residing on the anionic Bi-dimer as either Bi 6s, PDC π, or NO_3 orbitals. This electronic structure is confirmed by rendering of the frontier molecular orbitals (Figure 12), where the HOMOs are located on the Bi-dimer and the LUMOs on the R-Phen cation. As such, charge or electron transfer to the R-Phen from the Bi-dimer would appear favorable for **1-5** as this pathway facilitates negative charge from an electron rich donor to an electron poor acceptor. Notably, we draw attention to the calculated optical band gaps of **1-5** at 3.56 eV, 4.16 eV, 2.99 eV, 2.88 eV, and 3.21 eV, respectively. Here, the fluorescence-based compounds (**3** and **4**) feature the smallest band gap energies (< 3 eV) while the largest values belong to the phosphorescence-based **1** and **2**. Compound **5** has an intermediate band gap energy, displaying both fluorescence and phosphorescence behavior. The trend of band gap energy with the form

of photoluminescence implicates orbital overlap as the driver in emission, which is further supported by experimental data showing small Stokes shift for **3-5**. Close inspection of the calculated frontier orbital energies (Table S11) reveals that this trend primarily arises from variations in the HOMO values where **3-5** have the highest energies and **1-2** feature the lowest energies in the series, i.e. the phosphorescent compounds have more stable Bi-PDC MOs. The small band gaps for **3** and **4** are consistent with the weak emission displayed by the compounds; the emission at 430 nm (2.88 eV) is very close to the band gap energies (2.99 and 2.88 eV, respectively), suggesting that thermal deactivation of the excited state may occur between energy transfer states.

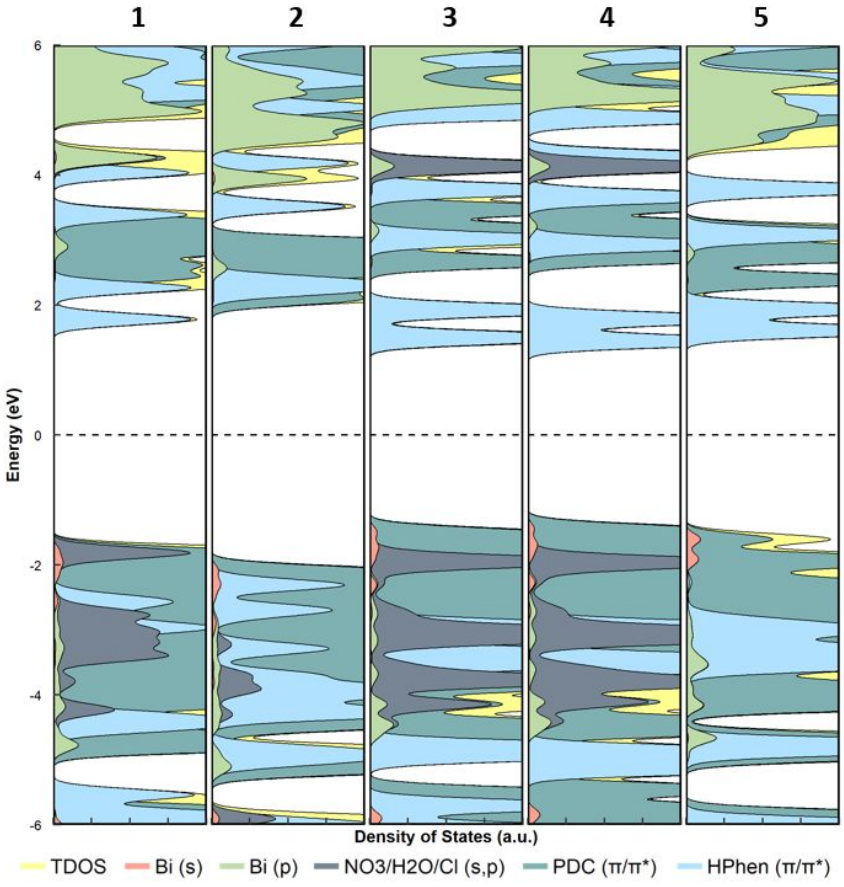

Fig. 11. Calculated total density of states (TDOS) of **1-5** and partial density of states (PDOS) projected onto atomic orbitals of Bi (s- and p-states), PDC (s- and p-states), $NO_3/H_2O/Cl$ (s- and p-states) and R-Phen (s- and p-states). Dashed line represents the Fermi level.

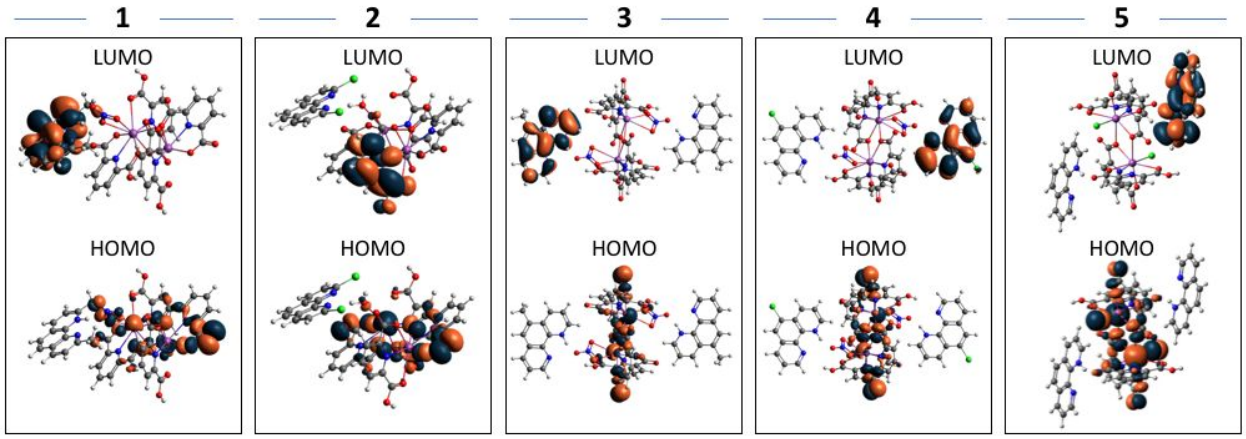

Fig. 12. Isodensity representations of frontier molecular orbitals of **1-5**. The HOMOs consist of BiPDC Bi 6s/PDC π orbitals while the R-phen π* comprises the LUMOs.

The excitation mechanisms of **1-5** were probed utilizing time-dependent DFT (TD-DFT) calculations for both singlet and triplet transitions. For these models, 'bright excited singlet states' are defined by f-oscillator strength values larger than 0.01. Full results of singlet and triplet excited states are found in Tables S12-S14. As a representative example, excited state calculations for **1** predict a bright excited singlet state at 330 nm (3.75 eV), well in agreement with the experimental excitation spectra. Dominant molecular orbital renderings (contributions > 10%) for this transition are shown in Figure 13. Here, the donor orbitals HOMO-8, HOMO-10, HOMO-11, and HOMO-12 originate energetically well below the HOMO and reside on both the anionic Bi-dimeric unit and the Me_2PhenH cation. For the Bi-dimer these orbitals primarily consist of PDC lone pair orbitals (p) and π orbitals while the Me_2PhenH

donor orbitals are bonding π orbitals. The acceptor orbitals LUMO and LUMO+1 strictly reside on the Me_2PhenH cation as π* orbitals. Similar transitions are observed in TD-DFT calculations of **2**-**5** despite the differences in organic units and charge. The long lifetimes found for **1**, **2**, and **5** point to intersystem crossings indicative of triplet state population and thus warrant investigation. Triplet state energies and transitions were calculated to confirm that these states energetically lie below the bright singlet states and share similar acceptor orbitals. As a representative, the bright excited triplet state of **1** is shown in Figure 14. This state occurs at 431 nm (2.8755 eV), much lower in energy compared to the lowest singlet state at 330 nm. Further, the acceptor molecular orbitals (LUMO and LUMO+1) are the same as the singlet state being composed of the R-Phen π*. This behavior is observed for all remaining compounds. Overall, the electronic mapping and TD-DFT findings point to favorable conditions for population of the organic R-Phen unit during excitation in **1**-**5** either through (i) a M/LLCT between Bi-dimers and R-Phen units or (ii) localized transitions from the R-Phen π/π* molecular orbitals. These results are consistent with experimental data showing R-Phen based emissions in **1**, **2**, and **5** but are inconclusive as to whether excited state population proceeds via TET or a photoinduced electron transfer and fail to explain the PDC-based fluorescence in **3** and **4**.

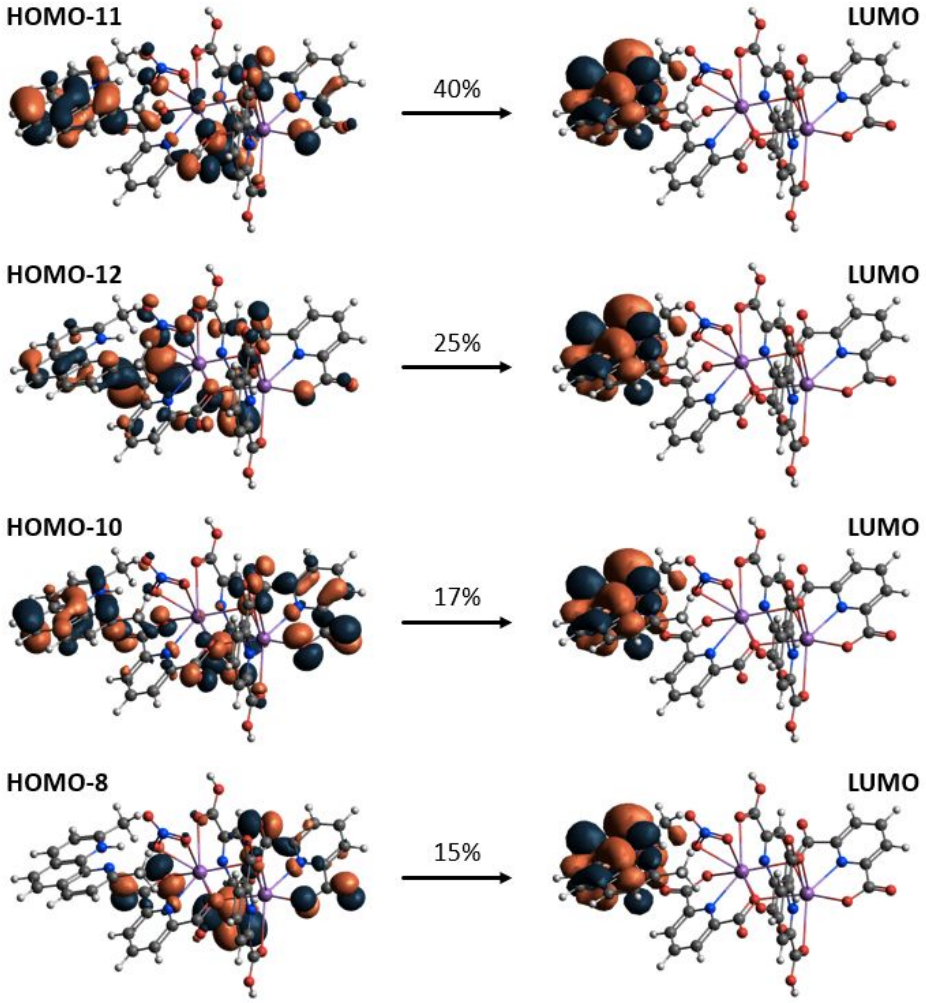

Fig. 13. TD-DFT calculated dominant orbital transitions for the lowest bright excited singlet state of **1** at 330 nm (3.7536 eV) showing BiPDC Bi 6s/PDC π and R-Phen π donor orbitals with phen π* acceptors.

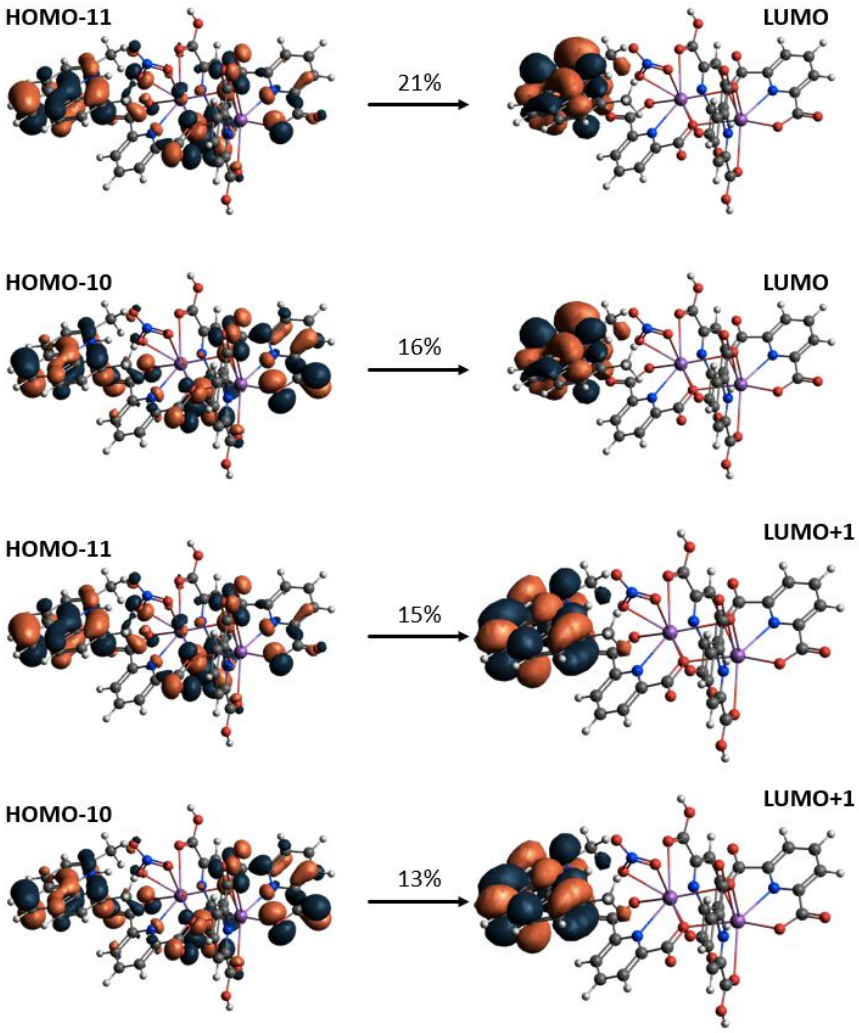

Fig. 14. TD-DFT calculated dominant orbital transitions for the lowest bright excited triplet state of **1** at 431 nm (2.8755 eV).

Changes in Free Energy and Rehm-Weller Analysis

To determine whether a photoinduced electron transfer mechanism is energetically feasible, changes in free energy of a photoinduced reaction where an electron is donated by the Bi-PDC unit and accepted by the organic phen were examined. The following elementary reactions (**1**) and (**2**) were considered:

$$[\text{Bi - PDC}]_1^0 + [\text{Phen}]_1^0 + h\nu \rightarrow [\text{Bi - PDC}]_3^{0*} + [\text{Phen}]_1^0 \quad (1)$$

$$[\text{Bi - PDC}]_3^{0*} + [\text{Phen}]_1^0 \rightarrow [\text{Bi - PDC}]_2^{+1} + [\text{Phen}]_2^{-1} \quad (2)$$

where $[\text{Bi - PDC}]_1^0$ and $[\text{Phen}]_1^0$ are the dimeric Bi-PDC and R-Phen units in the singlet ground state, respectively, $[\text{Bi - PDC}]_3^{0*}$ is the Bi-PDC excited triplet state, and $[\text{Bi - PDC}]_2^{+1}$ and $[\text{Phen}]_2^{-1}$ are oxidized and reduced doublet states, respectively. In reaction (**1**) the Bi-PDC unit undergoes a photoinduced change in spin state from singlet to triplet, the R-phen is unchanged. This is followed by the redox reaction (2) wherein an electron transfer from the triplet Bi-PDC to the singlet R-Phen occurs leaving doublet Bi-PDC and R-phen products. Total energies of the isolated units in the various multiplicities and charged states were calculated to determine the overall ΔG values (Table S16). As shown in Figure 15, conversion of the Bi-PDC unit from the singlet to the triplet state is endothermic and has at minimum a ΔG of +258 kJ/mol (**5**), well below the experimental excitation energies 350-380 nm (342-315 kJ/mol). From an excited Bi-PDC triplet state, transfer of an electron to the R-Phen unit via a redox reaction proceeds exothermically and is thermodynamically favorable where the energy difference ranges from -266.5 kJ/mol (**1**) to -575 kJ/mol (**2**). For **2**-**5**, the redox doublet products are predicted to be more stable than the initial singlet reactants by 227 kJ/mol while for **1** they are less stable by a modest 6.5 kJ/mol. The ΔG values clearly indicate that photo-reduction and -oxidation of the Bi-PDC and R-Phen units, respectively, is energetically feasible where the final state may serve as a meta-stable state.

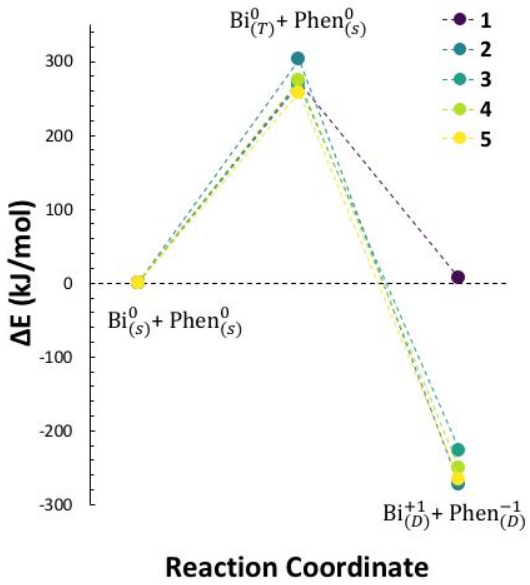

Fig. 15. Calculated changes in free energy for a photoinduced electron transfer between the Bi-PDC and organic R-Phen units of **1**-**5**. Changes in charge are superscripted and multiplicity (S- singlet, D – doublet, T- triplet) subscripted.

A Rehm-Weller analysis,[55, 56] which incorporates both theoretical and experimental data, was also performed to further support a photoinduced electron transfer using equation (**3**),

$$\Delta G_{ET} = (E_{ox} - E_{red}) - E_s - e_0^2/\varepsilon_a \quad (3)$$

where the change in energy of an electron transfer (G_{ET}) is a function of the reduction potential of Bi-PDC (E_{red}), the oxidation potential of the R-Phen (E_{ox}), the energy of the complex excited singlet state (E_s), and the coulombic attraction between the donor/acceptor pair (e_0^2/ε_a = 0.15 eV (+1/-1) and 0.06 eV (0/0)). The E_{ox} and E_{red} values for the Bi-PDC and R-Phen units were calculated from the DFT predicted changes in free energy while E_s was extracted from Tauc plots calculated from experimental diffuse reflectance spectra using the Kubelka-Munk theory (Figures S34-S38). Tauc plots can provide an estimation of the optical

band gap in semiconductors; to this end, a Tauc plot can be used to determine an experimental optical band gap for comparison to the computationally determined band gaps.[57] Rehm-Weller parameters are summarized in Table S17. The ΔG_{ET} values obtained are negative in all cases, ranging from -12.71 eV (**1**) to -1.95 eV (**2**), indicating that electron transfer is again thermodynamically favorable in **1-5**.

Rationalizing Photophysical Mechanism

The computational results support photoinduced electron transfer in compounds **1**, **2**, and **5** which display phosphorescent R-Phen emission, $^3\pi^*_{phen} \rightarrow {}^1\pi_{phen}$. Here, the molecular orbital conditions are favorable for excited state population of R-Phen given the low-lying unoccupied R-Phen π* orbitals and high lying occupied Bi 6s and PDC π orbitals. TD-DFT calculations, furthermore, predict that the R-Phen π* orbitals readily act as acceptors during excitation in both the lowest singlet and triplet states. Importantly, thermodynamic calculations via DFT calculated changes in free energy and the Rehm-Weller analysis reveal favorable conditions for formal electron transfer between Bi-PDC (donor) and R-Phen (acceptor) units. We would be remiss; however, to not consider direct excitation and emission of the R-Phen molecule as a probable emission pathway. The experimental emission of **1**, **2**, and **5** shows little to no deviation from that expected for the free R-Phen derivatives at low temperatures; no significant changes in λ_{max} nor profile are observed. This suggests that the orbitals of R-Phen are not significantly affected by those of the $Bi_2(HPDC)_2(PDC)_2$ dimer. Furthermore, the corresponding excitation bands are not similar to those expected for the free R-Phen; our observed λ_{max} of excitation is significantly lower in energy.[58] This

precludes the possibility that excitation follows an isolated $^1\pi_{phen} \rightarrow {}^1\pi^*_{phen}$ mechanism, leaving only photoinduced electron transfer as the most probable pathway for R-Phen phosphorescence. A generalized mechanism for photoinduced electron transfer for **1** and **2** is proposed in Figure 16.

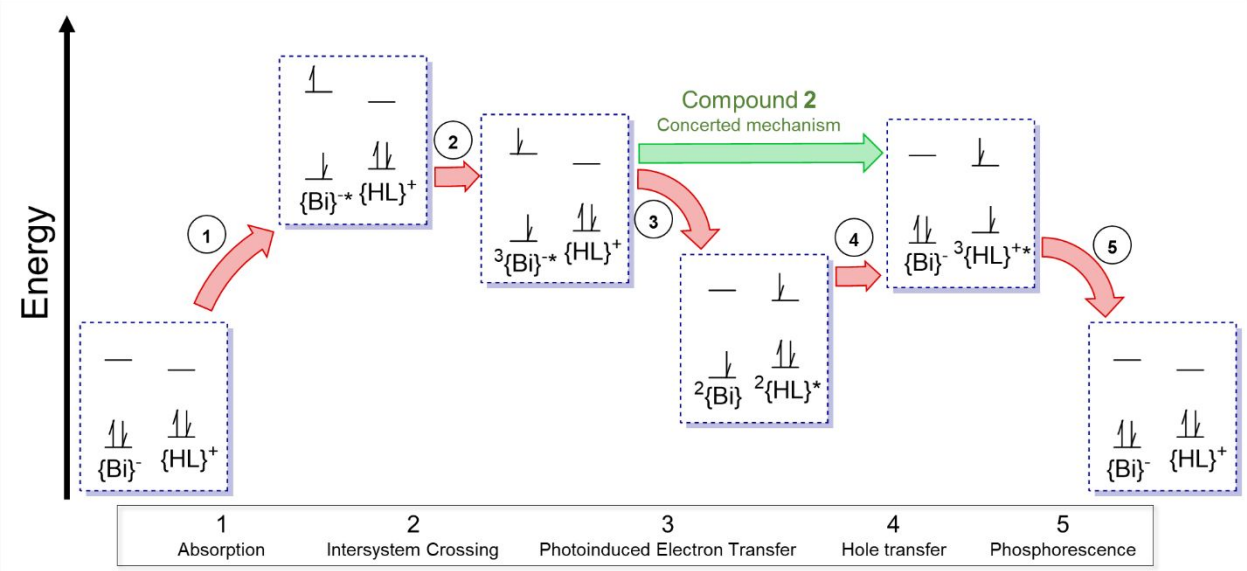

Fig. 16. Proposed photoinduced electron transfer mechanism for **1** and **2** tracking the movement of an electron. Each box contains a generalized orbital diagram for the dimer, {Bi}, and the N-heterocycle, {HL}, showing the transfer of electrons through the system. Compound **1** follows the red arrows exclusively and **2** follows the red arrows until it diverges at the green arrow due to a concerted electron transfer mechanism.

The computationally determined mechanism ut supra fails to fully explain; however, the fluorescence behavior in **3**, **4**, and **5**. These compounds also feature molecular orbital constructs and thermodynamic conditions suitable for formal electron transfer. Yet electron or triplet energy transfer behavior does not manifest experimentally, instead PDC-based emission is observed. Importantly, there is little variation in the excitation bands of **1-5** as compared to the emission bands where the PDC emission is significantly blue shifted compared to R-Phen. The result is an exceptionally small Stokes shift and

appreciable overlap of the excitation and emission bands. These observations point towards small energy differences between the excited and ground states where a secondary electron pathway is present that outcompetes excited state population of the R-Phen unit. These compounds are distinct in two primary ways: (i) the Bi center is stereochemically inactive and (ii) the R-Phen units do not feature noncovalent interactions. The ns^2 lone pair of group 4A-6A elements is known to heavily influence the photophysical properties of inorganic and hybrid materials.[59-61] For example, in perovskite derivatives, the carrier-phonon interaction increases with lone pair activity giving rise to low energy tailing in the emission as well as breaking of inversion symmetry towards ferroelectricity.[62, 63] Further, in a bismuth-halide hybrid system that displayed XMLCT, the energy of the HOMO was found to decrease with increasing lone pair stereochemical activity, thus increasing the band gap similarly to **1** and **2**.[53] As we are only just beginning to understand this class of materials, we are left to posit that expression of the Bi 6s lone pair electrons is partially responsible for the deviation in behavior.

Structure-Property Relationships

There exists a stark divergence in noncovalent interactions between the fluorescent and phosphorescent compounds, in addition to the previously mentioned differences in the stereochemical activity of the $6s^2$ lone pair. The differences in the structural chemistry likely arise from steric and supramolecular interactions promoted by the different phenanthroline derivatives. For example, compounds **3** and **4** have substitutions at the 5-position of the R-Phen, which likely results in increased steric

interactions with neighboring dimers in the extended crystal structure. Similarly, the π-π interactions of **1** and **2** show different interaction strengths; **2** displays shorter π-π distances, consistent with the presence of electron withdrawing substituents on the ring thus reducing electron density in the π-orbitals and reducing π-π repulsion between ligands. To this end, it is clear that introducing electron withdrawing and electron donating substituents onto the R-Phen directly determines the observed structure and thus properties.

Compounds **1**, **2** and **5** all exhibit strong π-π interactions between the R-Phen and 2,6-PDC, while **3** and **4** have no such Phen···PDC interactions. As such, Phen···PDC interactions appear to be important towards phosphorescence, as the excitation pathways for **1** and **2** suggest a formal electron transfer occurs from the dimeric substructure to the outer coordination R-Phen. It has been shown that through-space electron transfer processes are distance dependent.[64-66] The π-π interactions may help promote the close distance required to achieve the electron transfer to the phen derivative, or the electron transfer may proceed through the π orbitals of the PDC and R-Phen. Regardless, the observed correlation between phosphorescence and π-π stacking interactions in this work implies a dependence upon the interaction in stabilizing or promoting long-lived phosphorescence. The rate of charge transfers through π-coupled molecular systems is distance dependent, with one study showing a ~20-fold increase in the rate of charge transfer when changing from inter-ring distances of 4.0 Å to 3.0 Å;[67] compounds **1**, **2** and **5** each contain inter-ring distances within this range, with **2** displaying the shortest distance (3.562 Å) and **5** displaying the longest (3.772 Å). Further electron transfers promoted by π-π interactions have been observed in

nitrobenzene and trinitrotoluene sensors, although the electron transfers in these examples result in fluorescence quenching rather than promoting phosphorescence.[68-70] We originally entertained the idea that LP-π interactions could be responsible for promoting the electron transfer; however, compound **5** has no such interaction yet still displays long-lived PhenH phosphorescence.

Additional structural features further differentiate **1** and **2**; the most obvious difference is the presence of a nitrate capping **1** and a water ligand capping **2**. This further differentiates the hydrogen bonding interaction between the two compounds; **1** has a strong N-H···O interaction with a D···A distance of 2.738(9) Å while **2** has a weaker O-H···N interaction with a D···A distance of 2.924(7) Å. The introduction of hydrogen bonding interactions in cocrystals has been shown to increase the observed photoluminescent lifetime.[71] Yet the role that hydrogen bonding plays on the observed photoluminescence was not fully elucidated from this current study.

The information gleamed from this work regarding the effect that π-π interactions play on promoting phosphorescence, as well as the effect of charged versus neutral species on luminescence lifetimes, may provide guidelines with which supramolecular interactions may be used to achieve desired material properties. Such knowledge regarding properties that lead to radioluminescence, phosphorescence over fluorescence, tunability of lifetimes, or electron transfer processes is vital towards targeting specific applications.

CONCLUSION

Five photoluminescent bismuth(III)-organic materials were synthesized. Upon UV excitation, two of the compounds exhibited phosphorescence attributed to an outer coordination sphere fluorophore, two displayed purely fluorescence from a metal-coordinated ligand, and one showed both fluorescence and phosphorescence. Further, the phosphorescent compounds were found to emit visible light upon X-ray irradiation. Structure analysis suggested that the Bi lone pair as well as strong π-π interactions between the R-Phen and 2,6-PDC present in the phosphorescent compounds promoted electron transfers leading to room temperature phosphorescence, while the absence of these features resulted in fluorescence. Electronic structure and TD-DFT calculations were used to support a formal electron transfer assignment in phosphorescent compounds but fails to fully explain the fluorescence behavior observed in others. The compounds reported herein, demonstrate that subtle changes in the organic unit can drive dramatic shifts in structural and optical properties. As a family of materials, we are actively exploring new related compounds to probe and understand the underlying structure-property relationship.

EXPERIMENTAL SECTION

Materials

$Bi(NO_3)_3{\cdot}5H_2O$ (Fisher, 99.2%), $BiCl_3$ (Sigma-Aldrich, ≥98%), 1,10-phenanthroline (Acros Organics, 99+%), 2,9-dimethyl-1,10-phenanthroline hemihydrate (Alfa Aesar, 98+%), 2,9-dichloro-1,10-

phenanthroline (TCI Chemical, ≥97%), 5-methyl-1,10-phenanthroline hydrate (TCI Chemical, ≥98%), 5-chloro-1,10-phenanthroline (Alfa Aesar), 2,6-pyridinedicarboxylic acid (Alfa Aesar, 98%), nitric acid (Sigma-Aldrich, 70%), hydrochloric acid (Fisher Chemical, 36.5-38.0%), acetonitrile (Fisher Chemical, 99.98%) and ethanol (Warner Graham Company) were used as received. Nanopure water was utilized for all experiments (≤0.05 μS; Millipore, USA). 2,9-Dichloro-1,10-phenanthroline was weighed out in a vial in a nitrogen glovebox, capped, then removed from the glovebox for synthesis under ambient conditions.

Synthesis

2,9-Me_2PhenH[$Bi_2(HPDC)_2(PDC)_2(NO_3)$]·4$H_2O$ (1)

2,6-Pyridinedicarboxylic acid (0.0334 g, 0.20 mmol), and 2,9-dimethyl-1,10-phenanthroline hemihydrate (0.0434 g, 0.20 mmol) were dissolved in 1.5 mL ethanol via sonication in a 7.5 mL glass vial. In a separate vial, bismuth nitrate (0.0243 g, 0.05 mmol) was dissolved in 2M nitric acid (0.5 mL) and then diluted with an additional 1 mL aliquot of water. The ethanolic ligand solution was then gently layered onto the bismuth nitrate solution. The vial was capped and allowed to sit at room temperature. After three days, crystals had formed and the solvent was then removed. The product was collected, washed with ethanol, and allowed to dry under ambient conditions. Two phases had precipitated from solution: colorless rectangular plates that exhibited blue-green luminescence under a UV lamp (compound **1**), as well as sparse, large, non-luminescent block crystals of a previously reported phase, $Bi_2(HPDC)_2(PDC)_2(H_2O)_2 \cdot 5H_2O$.[72] The non-luminescent block crystals were manually removed leaving **1** as a pure phase. Yield: 48% (based on Bi). Elemental Analysis for $C_{42}H_{35}Bi_2N_7O_{23}$: Calc. (Obs.): C, 35.4 (35.2); H, 2.5 (2.4); N, 6.9 (6.8%).

The reaction was scaled up 10-fold by adding a 15 mL ethanolic solution of 2,9-dimethyl-1,10-phenanthroline (2.00 mmol; 0.4340 g) and 2,6-pyridinedicarboxylic acid (2.00 mmol; 0.3340 g) to a stirring

solution of bismuth nitrate pentahydrate (0.50 mmol; 0.2430 g) dissolved in 5 mL 2M nitric acid diluted with an additional 10 mL water. Product formation was evident within 15 seconds and yielded bright blue luminescent slurry. The reaction was allowed to continue for two hours, after which the mixture was vacuum filtered and rinsed with ethanol, yielding a pure phase upon drying. Yield: 99.1% (based on Bi).

2,9-Cl_2Phen[Bi_2(HPDC)$_2$(PDC)$_2$(H_2O)]·4H_2O (2)

2,6-Pyridinedicarboxylic acid (0.0334 g, 0.20 mmol), and 2,9-dichloro-1,10-phenanthroline (0.0498 g, 0.20 mmol) were dissolved in 1.5 mL ethanol via sonication in a 7.5 mL glass vial. In a separate vial, bismuth nitrate (0.0243 g, 0.05 mmol) was dissolved in 2M nitric acid (0.5 mL) and then diluted with an additional 1 mL aliquot of water. The ethanolic solution was added to the aqueous solution and vortexed for thirty seconds. The vial was then allowed to sit undisturbed at room temperature. After seven days, a blue luminescent phase had precipitated on the bottom of the vial, along with a thick, white powder, presumably precipitated dichlorophenanthroline. The product was filtered, washed with water, ethanol, and four aliquots of dichloromethane and allowed to dry under ambient conditions. Upon rinsing with dichloromethane, a DCM-adduct of the desired product was isolated from the filter paper as colorless rectangular plates that exhibited blue luminescence under a UV lamp as a pure phase. Yield: 41% (based on Bi). Elemental Analysis of the DCM rinsed product was consistent for $C_{80}H_{60}Bi_4N_{12}O_{42}Cl_4 \cdot CH_2Cl_2$: Calc. (Obs.): C, 33.3 (33.2); H, 2.1 (2.2); N, 5.8 (5.5%).

(5-MePhenH)$_2$[Bi_2(HPDC)$_2$(PDC)$_2$(NO_3)$_2$]·6H_2O (3)

2,6-Pyridinedicarboxylic acid (0.0334 g, 0.20 mmol), and 5-methyl-1,10-phenanthroline hydrate (0.0388 g, 0.20 mmol) were dissolved in 1.5 mL ethanol via sonication in a 7.5 mL glass vial. In a separate vial, bismuth nitrate (0.0243 g, 0.05 mmol) was dissolved in 2M nitric acid (0.5 mL) and then diluted with an additional 1 mL aliquot of water. The ethanolic ligand solution was then gently layered onto the bismuth nitrate solution. The vial was capped and allowed to sit at room temperature. After two days, crystals of **3** had formed and the solvent was then removed. The product was collected, washed with 1-propanol, and

allowed to dry under ambient conditions. Colorless rectangular plates that exhibited purple luminescence under a UV lamp were isolated as a pure phase. Yield: 32% (based on Bi). Elemental Analysis for $C_{54}H_{48}Bi_2N_{10}O_{28}$: Calc. (Obs.): C, 38.1 (37.7); H, 2.8 (2.6); N, 8.2 (8.1%).

(5-ClPhenH)$_2$[Bi$_2$(HPDC)$_2$(PDC)$_2$(NO$_3$)$_2$]·6H$_2$O (4)

Crystals suitable for single crystal x-ray diffraction were obtained for **4** by performing an identical reaction to that described for **3** but with 5-chloro-1,10-phenanthroline. However, an unknown impurity was observed via powder X-ray diffraction.

To obtain **4** as a pure phase, 2,6-pyridinedicarboxylic acid (0.0334 g, 0.20 mmol), and 5-chloro-1,10-phenanthroline (0.0429 g, 0.20 mmol) were dissolved in 1.5 mL ethanol via sonication in a 7.5 mL glass vial. In a separate vial, bismuth nitrate (0.0243 g, 0.05 mmol) was dissolved in 2M nitric acid (0.5 mL) and then diluted with an additional 1 mL aliquot of water. The ethanolic solution was added to the aqueous solution and the mixture was stirred for 17 hours under ambient conditions. The reaction was then filtered and the solids were rinsed with ethanol and dichloromethane, and then allowed to dry. The product was isolated as a white powder that exhibited purple luminescence under a UV lamp. Yield: 75% (based on Bi). Elemental Analysis for $C_{52}H_{42}Bi_2N_{10}O_{28}Cl_2$: Calc. (Obs.): C, 35.8 (35.5); H, 2.4 (2.3); N, 8.0 (7.8%).

(PhenH)$_2$[Bi$_2$(HPDC)$_2$(PDC)$_2$Cl$_2$]·8H$_2$O (5)

2,6-Pyridinedicarboxylic acid (0.0334 g, 0.20 mmol), and 1,10-phenanthroline (0.0360 g, 0.20 mmol) were dissolved in 1.5 mL ethanol via sonication in a 7.5 mL glass vial. In a separate vial, bismuth nitrate (0.0243 g, 0.05 mmol) was dissolved in 2M hydrochloric acid (0.5 mL) and then diluted with an additional 1 mL aliquot of water. The ethanolic ligand solution was then gently layered onto the bismuth nitrate solution and the vial was capped. A precipitate immediately formed, yet the reaction was allowed to sit at room temperature. After three days, crystals had formed and the solvent was then removed. The product was collected, washed with ethanol, and allowed to dry under ambient conditions. Two phases had precipitated from solution: large block crystals that exhibited blue-green luminescence under a UV lamp (compound **5**),

as well as unidentified, non-photoluminescent microcrystalline solids. The luminescent block crystals were manually transferred to a clean vial, and **5** was isolated as a phase pure product. Yield: 24% (based on Bi). Elemental Analysis for $C_{52}H_{48}Bi_2N_8O_{24}Cl_2$: Calc. (Obs.): C, 37.7 (37.9); H, 2.9 (2.7); N, 6.8 (6.7%).

Structure Determination via Single Crystal X-ray Diffraction

Single crystals of **1-5** were isolated from the bulk and mounted on a MiTeGen micromount in N-paratone. Single crystal X-ray diffraction data for **1**, and **3-5** were collected at 100 K on a Bruker D8 Quest diffractometer equipped with an I*u*S X-ray source (Mo-Kα radiation; λ=0.71073 Å) and a Photon 100 detector. Diffraction data for **2** were collected at 100 K on a Bruker APEX Duo diffractometer equipped with a fine-focus sealed tube source (Mo-Kα radiation; λ=0.71073 Å) and an APEX II CCD detector. Data were integrated using the SAINT software package included with APEX3.[73, 74] An absorption correction was applied using a multi-scan technique in SADABS.[75] The structure was solved using intrinsic methods via SHELXT and refined by full-matrix least-squares on F2 using the SHELXL software in shelXle64.[76, 77] Crystallographic data for **1-5** is provided in Table 1, and the resulting CIF data are available as Supporting Information. Crystallographic data was deposited in the Cambridge Crystallographic Data Centre (CCDC) and may be found at http://www.ccdc.cam.ac.uk/ by using reference numbers 2252252-2252256.

Table 1. Crystallographic Structure Refinement Details for compounds **1-5**.

	1	**2**	**3**	**4**	**5**

Formula	$C_{42}H_{35}Bi_2N_7O_{23}$	$C_{40}H_{30}Bi_2N_6O_{21}Cl_2$	$C_{54}H_{48}Bi_2N_{10}O_{28}$	$C_{52}H_{42}Bi_4N_{10}O_{28}Cl_2$	$C_{52}H_{48}Bi_2N_8O_{24}Cl_2$
MW ($gmol^{-1}$)	1423.73	1419.56	1702.98	1743.81	1657.84
T (K)	100	100	100	100	100
λ (K α)	0.71073	0.71073	0.71073	0.71073	0.71073
μ (mm^{-1})	8.046	8.198	6.281	6.448	6.615
Crystal System	Triclinic	Triclinic	Triclinic	Triclinic	Triclinic
Space Group	*P*-1	*P*-1	*P*-1	*P*-1	*P*-1
a (Å)	9.3536(4)	9.121(2)	9.1883(7)	9.204(1)	10.0241(4)
b (Å)	12.0494(6)	12.323(3)	11.512(1)	11.493(1)	11.9736(5)
c (Å)	21.237(1)	21.183(5)	14.948(2)	14.771(2)	13.5032(6)
α (°)	87.192(1)	85.845(3)	72.800(3)	72.918(4)	112.431(1)
β (°)	84.025(1)	83.706(3)	78.455(3)	78.693(3)	111.637(1)
γ (°)	68.322(1)	68.570(3)	71.506(3)	71.408(3)	91.059(1)
Volume ($Å^3$)	2212.0(2)	2201.5(8)	1422.6(3)	1406.5(3)	1368.4(1)
Z	2	2	1	1	1
R_{int}	0.0516	0.0420	0.0264	0.0305	0.0296
R ($I > 2\sigma$)	0.0390	0.0272	0.0163	0.0201	0.0137
wR_2	0.0864	0.0632	0.0352	0.0398	0.0354
GooF	1.050	1.024	1.072	1.082	1.119
Residual density (max/min) ($e \cdot Å^{-3}$)	5.60 and -1.53	0.95 and -1.12	0.80 and -0.73	1.11 and -0.70	0.63 and -1.13
CCDC No.	2252252	2252256	2252253	2252254	2252255

Characterization methods

Powder patterns were obtained for the reaction products that yielded **1-5** using Cu-Kα radiation (λ = 1.542 Å) on a Rigaku Ultima IV X-ray diffractometer from 3-40˚ in 2θ with a step speed of 1 degree/min (Figures S13-S17). Combustion elemental analysis was performed using a Perkin Elmer Model 2400 Elemental Analyzer on the bulk phase. Thermogravimetric analysis was collected using a TA Instruments Q50

Thermogravimetric Analyzer under flowing N_2 at a temperature ramp rate of 5 °C per minute (Figure S18-S22). Diffuse reflectance spectra were collected using an OceanOptics DH-2000-BAL light source with a fiber optic probe (Figure S30-S34).

Photoluminescence

Excitation and emission spectra were collected on a Horiba PTI QM-400 spectrofluorometer on ground solid sample pressed between two quartz microscope slides at room temperature with 1-2 nm spectral widths. Lifetime measurements were collected with a lamp frequency of 100 Hz and exponential decay curves were fit with OriginPro 8.5. For compounds **1-2**, a 400 nm longpass filter was used to avoid harmonic peaks from the excitation source. CIE chromaticity coordinates were calculated in MATLAB from emission spectra for excitation-based color tuning studies.[78] Low temperature luminescent spectra were collected by immersing NMR tubes containing the powders in liquid nitrogen at 77 K using a Cold Finger Dewar K-158 attachment for the fluorometer.

Computational Methods

Molecular DFT modeling was performed using the Gaussian 16 package (Gaussian Inc). Calculations were executed on neutral models built from dimeric anionic Bi units charge balanced by organic cations truncated from experimental crystallographic structures. The B3LYP[79, 80] functional with the 6-311G(d,p)[81, 82] basis set from C/H/N/O and the modified scalar-relativistic effective core potential (ECP) bases set DEF2TZVP[83,

[84] with associated pseudopotentials for Bi/Cl atoms were used as implemented in the software. Optimization of calculated ground states were validated via harmonic frequency analysis ensuring no remaining imaginary frequencies. Calculated ground state parameters and TD-DFT transitions are provided as Supporting Information. Molecular orbitals were rendered from the derived wavefunction using the Avogadro software package (v1.2.0).[85] Changes in free energy were obtained from isolated anionic and cationic units with optimization.

Radioluminescence

Radioluminescence measurements were carried out on a customer-designed configuration of the Freiberg Instruments Lexsyg Research spectrofluorometer equipped with a Varian Medical Systems VF-50J X-ray tube with a tungsten target. The X-ray source was coupled with a Crystal Photonics CXD-S10 photodiode for continuous radiation intensity monitoring. The light emitted by the sample was collected by an Andor Technology SR-OPT-8024 optical fiber connected to an Andor Technology Shamrock 163 spectrograph coupled to a cooled (-80 °C) Andor Technology DU920P-BU Newton CCD camera (spectral resolution of ~0.5 nm/pixel). Radioluminescence was measured under continuous X-ray irradiation (W lines and bremsstrahlung radiation; 40 kV, 1 mA) with an integration time of 1 s. Powdered samples filled ~8 mm diameter, 0.5 mm deep cups, thus allowing for relative radioluminescence intensity comparison between different samples using bismuth germanium oxide (BGO) powder (Alfa Aesar Puratronic, 99.9995% (metals basis)) as a reference. Comparison was done by integrating the spectra from 350 to 750 nm, with

percentages being given in relation to the integrated signal of the BGO powder. Spectra were automatically corrected using the spectral response of the system determined by the manufacturer.

ASSOCIATED CONTENT

Supporting Information

The Supporting Information is available free of charge: crystallographic refinement details, ORTEP diagrams for **1-5**, supramolecular packing diagrams, powder X-ray diffraction plots, thermogravimetric analysis data, variable temperature luminescence spectra, phosphorescence decay plots, diffuse reflectance spectra, noncovalent interaction tables, and additional computational analysis information.

Accession Code

CCDC 2252252-2252256 contains the supplementary crystallographic data for this paper. These data can be obtained free of charge via www.ccdc.cam.ac.uk/data_request/cif, or by emailing data_request@ccdc.cam.ac.uk, or by contacting The Cambridge Crystallographic Data Centre, 12 Union Road, Cambridge CB2 1EZ, UK; fax: +44 1223 336033.

AUTHOR INFORMATION

Corresponding Author

*Karah E. Knope (kek44@georgetown.edu)

Author Contributions

The manuscript was written through contributions of all authors. All authors have given approval to the final version of the manuscript.

ORCID:

Alexander Marwitz: 0000-0002-2560-9184

Aaron D. Nicholas: 0000-0001-9003-2126

Anuj Dutta: 0000-0001-6896-7371

Joel Swanson: 0000-0002-3168-8579

Jeffery A. Bertke: 0000-0002-3419-5163

Jeffrey J. Rack: 0000-0001-6121-879X

Luiz G. Jacobsohn: 0000-0001-8991-3903

Karah E. Knope: 000-0002-5690-715X

Funding Sources

National Science Foundation (grants NSF DMR-2203658 and NSF DMR-1653016).

Notes

Any additional relevant notes should be placed here.

ACKNOWLEDGMENT

This work was supported by the National Science Foundation under grant NSF DMR-2203658. Luiz G. Jacobsohn's effort was supported by the National Science Foundation under grant NSF DMR-1653016.

REFERENCES

1. A. Garci, J. A. Weber, R. M. Young, M. Kazem-Rostami, M. Ovalle, Y. Beldjoudi, A. Atilgan, Y. J. Bae, W. Liu, L. O. Jones, C. L. Stern, G. C. Schatz, O. K. Farha, M. R. Wasielewski and J. Fraser Stoddart, *Nat. Catal.*, 2022, **5**, 524-533.
2. M. Liu, P. Xia, G. Zhao, C. Nie, K. Gao, S. He, L. Wang and K. Wu, *Angew. Chem. Int. Ed.*, 2022, **61**, e202208241.
3. C. Strauch, S. Schroeder, G. Grelier and M. Niggemann, *Chem. Eur. J.*, 2022, **28**, e202201830.
4. F. Strieth-Kalthoff, M. J. James, M. Teders, L. Pitzer and F. Glorius, *Chem. Soc. Rev.*, 2018, **47**, 7190-7202.
5. Y. Liu, C. Li, Z. Ren, S. Yan and M. R. Bryce, *Nat. Rev. Mater.*, 2018, **3**.
6. Y. Shi, Z. Wang, T. Meng, T. Yuan, R. Ni, Y. Li, X. Li, Y. Zhang, Z. Tan, S. Lei and L. Fan, *J. Am. Chem. Soc.*, 2021, **143**, 18941-18951.
7. Z. Xie, X. Zhang, H. Wang, C. Huang, H. Sun, M. Dong, L. Ji, Z. An, T. Yu and W. Huang, *Nat. Commun.*, 2021, **12**, 3522.
8. X. Jiang, Z. Dong, X. Miao, K. Wang, F. Yao, Z. Gao, B. Mi, Y. Yi, G. Yang and Y. Qian, *Adv. Func. Mat.*, 2022, **32**, 2205697.
9. N. Aizawa, A. Matsumoto and T. Yasuda, *Sci. Adv.*, **7**, eabe5769.
10. X. Y. Dong, Y. Si, J. S. Yang, C. Zhang, Z. Han, P. Luo, Z. Y. Wang, S. Q. Zang and T. C. W. Mak, *Nat. Commun.*, 2020, **11**, 3678.
11. L. Huang, T. Le, K. Huang and G. Han, *Nat. Commun.*, 2021, **12**, 1898.
12. A. M. Prokhorov, T. Hofbeck, R. Czerwieniec, A. F. Suleymanova, D. N. Kozhevnikov and H. Yersin, *J. Am. Chem. Soc.*, 2014, **136**, 9637-9642.
13. J. C. Koziar and D. O. Cowan, *Acc. Chem. Res.*, 1978, **11**, 334–341.
14. J. R. Ochola and M. O. Wolf, *Org. Biomol. Chem.*, 2016, **14**, 9088-9092.
15. V. W.-W. Yam, A. K.-W. Chan and E. Y.-H. Hong, *Nat. Rev. Chem.*, 2020, **4**, 528-541.
16. R. Lai, Y. Liu, X. Luo, L. Chen, Y. Han, M. Lv, G. Liang, J. Chen, C. Zhang, D. Di, G. D. Scholes, F. N. Castellano and K. Wu, *Nat. Commun.*, 2021, **12**, 1532.
17. X. Luo, Y. Han, Z. Chen, Y. Li, G. Liang, X. Liu, T. Ding, C. Nie, M. Wang, F. N. Castellano and K. Wu, *Nat. Commun.*, 2020, **11**, 28.
18. X. Luo, G. Liang, Y. Han, Y. Li, T. Ding, S. He, X. Liu and K. Wu, *J. Am. Chem. Soc.*, 2020, **142**, 11270-11278.
19. D. L. Dexter, *J. Chem. Phys.*, 1953, **21**, 836-850.
20. G. Porter and F. Wilkinson, *Proc. R. Soc. Lond. A*, 1961, **264**, 1-18.
21. J. Grosskopf, T. Kratz, T. Rigotti and T. Bach, *Chem. Rev.*, 2022, **122**, 1626-1653.
22. F. Strieth-Kalthoff and F. Glorius, *Chem*, 2020, **6**, 1888-1903.
23. J. Liao, W. Guo and X. Luo, *J. Photochem. Photobiol.*, 2022, **11**, 100128.
24. H. C. Brenner and C. A. Hutchison, *J. Chem. Phys.*, 1973, **58**, 1328-1342.
25. N. Swain and S. Mishra, *J. Clean. Prod.*, 2019, **220**, 884-898.
26. A. Varmazyari, A. Taghizadehghalehjoughi, C. Sevim, O. Baris, G. Eser, S. Yildirim, A. Hacimuftuoglu, A. Buha, D. R. Wallace, A. Tsatsakis, M. Aschner and Y. Mezhuev, *Toxicol. Rep.*, 2020, **7**, 637-648.
27. D. Volz, M. Wallesch, C. Fléchon, M. Danz, A. Verma, J. M. Navarro, D. M. Zink, S. Bräse and T. Baumann, *Green Chemistry*, 2015, **17**, 1988-2011.
28. J. C. Jin, N. N. Shen, Y. P. Lin, L. K. Gong, H. Y. Tong, K. Z. Du and X. Y. Huang, *Inorg. Chem.*, 2020, **59**, 13465-13472.
29. S. M. Parke, M. A. B. Narreto, E. Hupf, R. McDonald, M. J. Ferguson, F. A. Hegmann and E. Rivard, *Inorg. Chem.*, 2018, **57**, 7536-7549.
30. O. Toma, M. Allain, F. Meinardi, A. Forni, C. Botta and N. Mercier, *Angew. Chem. Int. Ed.*, 2016, **55**, 7998-8002.

31. O. Toma, N. Mercier, M. Allain, A. Forni, F. Meinardi and C. Botta, *Dalton Trans.*, 2015, **44**, 14589-14593.
32. L. G. Jacobsohn, M. W. Blair, S. C. Tornga, L. O. Brown, B. L. Bennett and R. E. Muenchausen, *J. Appl. Phys.*, 2008, **104**, 124303.
33. L. G. Jacobsohn, B. C. Tappan, S. C. Tornga, M. W. Blair, E. P. Luther, B. A. Mason, B. L. Bennett and R. E. Muenchausen, *Opt. Mater.*, 2010, **32**, 652-656.
34. R. L. Ayscue, V. Vallet, J. A. Bertke, F. Réal and K. E. Knope, *Inorganic Chemistry*, 2021, **60**, 9727-9744.
35. A. K. Adcock, R. L. Ayscue, L. M. Breuer, C. P. Verwiel, A. C. Marwitz, J. A. Bertke, V. Vallet, F. Real and K. E. Knope, *Dalton Trans.*, 2020, **49**, 11756-11771.
36. L. A. Maurer, O. M. Pearce, F. D. R. Maharaj, N. L. Brown, C. K. Amador, N. H. Damrauer and M. P. Marshak, *Inorg. Chem.*, 2021, **60**, 10137-10146.
37. M. K. Feyand, M.; Friedrichs, G.; Stock, N., *Chemistry - A European Journal*, 2013, **19**, 12537-12546.
38. L. Pan, K. Koehler and L. G. Jacobsohn, *J. Lumin.*, 2020, **228**, 117626.
39. M. Shimizu, M. Koshimizu, Y. Fujimoto, T. Yanagida, S. Ono and K. Asai, *Opt. Mater.*, 2016, **61**, 115-118.
40. I. Caracelli, I. Haiduc, J. Zukerman-Schpector and E. R. T. Tiekink, *Coord. Chem. Rev.*, 2013, **257**, 2863-2879.
41. A. C. Marwitz, A. D. Nicholas, L. M. Breuer, J. A. Bertke and K. E. Knope, *Inorg. Chem.*, 2021, **60**, 16840-16851.
42. L. Miersch, T. Rüffer, M. Schlesinger, H. Lang and M. Mehring, *Inorg. Chem.*, 2012, **51**, 9376-9384.
43. O. Anjaneyulu, T. K. Prasad and K. C. K. Swamy, *Dalton Trans.*, 2010, **39**, 1935-1940.
44. B. Lesniewska, O. Danylyuk, K. Suwinska, T. Wojciechowski and A. W. Coleman, *CrystEngComm*, 2011, **13**, 3265.
45. I. Dance, *New J. Chem.*, 2003, **27**, 22-27.
46. C. Janiak, *J. Chem. Soc., Dalton Trans.*, 2000, 3885-3896.
47. G. Accorsi, A. Listorti, K. Yoosaf and N. Armaroli, *Chem. Soc. Rev.*, 2009, **38**, 1690-1700.
48. D. Malyshev, R. Öberg, L. Landström, P. O. Andersson, T. Dahlberg and M. Andersson, *Spectrochim. Acta A*, 2022, **271**, 120869.
49. G. G. Giachino and D. R. Kearns, *J. Chem. Phys.*, 1970, **53**, 3886-3891.
50. W. Dai, X. Niu, X. Wu, Y. Ren, Y. Zhang, G. Li, H. Su, Y. Lei, J. Xiao, J. Shi, B. Tong, Z. Cai and Y. Dong, *Angew. Chem. Int. Ed.*, 2022, **61**.
51. X. Wang, H. Shi, H. Ma, W. Ye, L. Song, J. Zan, X. Yao, X. Ou, G. Yang, Z. Zhao, M. Singh, C. Lin, H. Wang, W. Jia, Q. Wang, J. Zhi, C. Dong, X. Jiang, Y. Tang, X. Xie, Y. M. Yang, J. Wang, Q. Chen, Y. Wang, H. Yang, G. Zhang, Z. An, X. Liu and W. Huang, *Nat. Photonics*, 2021, **15**, 187-192.
52. J. N. Demas and S. E. Demas, in *Reference Module in Chemistry, Molecular Sciences and Chemical Engineering*, Elsevier, 2014, DOI: https://doi.org/10.1016/B978-0-12-409547-2.11000-5.
53. R. L. Ayscue, V. Vallet, J. A. Bertke, F. Real and K. E. Knope, *Inorg. Chem.*, 2021, **60**, 9727-9744.
54. A. W. Kelly, A. M. Wheaton, A. D. Nicholas, F. H. Barnes, H. H. Patterson and R. D. Pike, *Eur. J. Inorg. Chem.*, 2017, **2017**, 4990-5000.
55. D. Rehm and A. Weller, *Isr. J. Chem.*, 1970, **8**, 259-271.
56. A. Weller, *Z. Phys. Chem.*, 1982, **133**, 93-98.
57. P. Makuła, M. Pacia and W. Macyk, *J. Phys. Chem. Lett.*, 2018, **9**, 6814-6817.
58. N. Yoshikawa, S. Yamazaki, Y. Kakimoto, S. Eguchi, R. Yokoyama, N. Kanehisa, N. Tohnai, E. Nakata and H. Takashima, *J. Mol. Struct.*, 2021, **1242**, 130728.

59. D. H. Fabini, G. Laurita, J. S. Bechtel, C. C. Stoumpos, H. A. Evans, A. G. Kontos, Y. S. Raptis, P. Falaras, A. Van der Ven, M. G. Kanatzidis and R. Seshadri, *J. Am. Chem. Soc.*, 2016, **138**, 11820-11832.
60. D. H. Fabini, R. Seshadri and M. G. Kanatzidis, *MRS Bull.*, 2020, **45**, 467-477.
61. K. M. McCall, V. Morad, B. M. Benin and M. V. Kovalenko, *ACS Mater. Lett.*, 2020, **2**, 1218-1232.
62. X. Li, Y. Guan, X. Li and Y. Fu, *J. Am. Chem. Soc.*, 2022, **144**, 18030-18042.
63. Y. Fu, S. Jin and X. Y. Zhu, *Nat. Rev. Chem.*, 2021, **5**, 838-852.
64. N. S. Hush, *Coord. Chem. Rev.*, 1985, **64**, 135-157.
65. M. Kuss-Petermann and O. S. Wenger, *Phys. Chem. Chem. Phys.*, 2016, **18**, 18657-18664.
66. K. J. Lee, Y. Xiao, E. S. Kim, F. Mathevet, L. Mager, O. Cregut, F. Frédéric, J.-C. Ribierre, J. W. Wu and A. D'Aléo, *ACS Photonics*, 2019, **6**, 2649-2654.
67. A. Batra, G. Kladnik, H. Vazquez, J. S. Meisner, L. Floreano, C. Nuckolls, D. Cvetko, A. Morgante and L. Venkataraman, *Nat. Commun.*, 2012, **3**, 1086.
68. M. Lu, P. Zhou, Z. Li, J. Liu, Y. Yang and K. Han, *Phys. Chem. Chem. Phys.*, 2018, **20**, 19539-19545.
69. M. Lu, P. Zhou, Y. Ma, Z. Tang, Y. Yang and K. Han, *J. Phys. Chem. A*, 2018, **122**, 1400-1405.
70. B. Sun, T. Tao, L. Liu, R. Ding and Y. Mao, *J. Phys. Chem. C*, 2021, **125**, 12433-12440.
71. B. Zhou and D. Yan, *Adv. Func. Mat.*, 2019, **29**, 1807599.
72. O. Anjaneyulu and K. C. Kumara Swamy, *J. Chem. Sci.*, 2011, **123**, 131-137.
73. *SAINT*, Bruker AXS Inc.: Madison, WI, USA, 2007.
74. *APEX3*, Bruker AXS Inc.: Madison, WI, USA, 2016.
75. *SADABS*, Bruker AXS Inc.: Madison, WI, USA, 2008.
76. G. Sheldrick, *Acta Crystallogr., Sect. A*, 2008, **64**, 112-122.
77. C. B. Hubschle, G. M. Sheldrick and B. Dittrich, *J. Appl. Crystallogr.*, 2011, **44**, 1281-1284.
78. P. Patil, *CIE Coordinate Calculator*, R2020a; The MathWorks Inc.: 2011.
79. A. D. Becke, *J. Chem. Phys.*, 1993, **98**, 5648-5652.
80. C. Lee, W. Yang and R. G. Parr, *Phys. Rev. B*, 1988, **37**, 785-789.
81. A. D. McLean and G. S. Chandler, *J. Chem. Phys.*, 1980, **72**, 5639-5648.
82. R. Krishnan, J. S. Binkley, R. Seeger and J. A. Pople, *J. Chem. Phys.*, 1980, **72**, 650-654.
83. F. Weigend, *Phys. Chem. Chem. Phys.*, 2006, **8**, 1057-1065.
84. F. Weigend and R. Ahlrichs, *Phys. Chem. Chem. Phys.*, 2005, **7**, 3297-3305.
85. M. D. Hanwell, D. E. Curtis, D. C. Lonie, T. Vandermeersch, E. Zurek and G. R. Hutchison, *J. Cheminform.*, 2012, **4**, 17.